Microbial Community Compositional Stability in Agricultural Soils During Freeze-Thaw and Fertilizer Stress

by

Grant Jensen

A thesis

presented to the University of Waterloo

in fulfillment of the

thesis requirement for the degree of

Master of Science

in

Biology

Waterloo, Ontario, Canada, 2024

Author's Declaration

This thesis consists of materials all of which I authored or co-authored: see Statement of Contributions included in the thesis. This is a true copy of the thesis, including any required final revisions, as accepted by my examiners. I understand that my thesis may be made electronically available to the public.

Statement of Contributions

Grant Jensen was the primary author for the work described in this thesis. The majority of the contents of this thesis have been published as “Microbial Community Compositional Stability in Agricultural Soils During Freeze-Thaw and Fertilizer Stress” (Jensen, G.J., Krogstad K., Rezanezhad F., & Hug, L.A., Frontiers Environmental Science 2022, DOI: https://doi.org/10.3389/fenvs.2022.908568). The experiment described was conducted jointly, including experimental setup, with Konrad Krogstad who produced the majority of the geochemical analysis described in Chapter 2.6.

Abstract

Microbial activity persists in cold region agricultural soils during the fall, winter, and spring (i.e., non-growing season) and frozen condition, with peak activity during thaw events. Climate change is expected to change the frequency of freeze-thaw cycles (FTC) and extreme temperature events (i.e, altered timing, extreme heat/cold events) in temperate cold regions, which may hasten microbial consumption of fall-amended fertilizers, decreasing potency come the growing season. In this thesis, I conducted a high-resolution temporal examination of the impacts of freeze-thaw and nutrient stress on microbial communities in agricultural soils across both soil depth and time. Four soil columns were incubated under a climate model of a non-growing season including precipitation, temperature, and thermal gradient with depth over 60 days. Two columns were amended with fertilizer, and two incubated as unamended soil. The impacts of repeated FTC and nutrient stress on bacterial, archaeal, and fungal soil community members were determined, providing a deeply sampled longitudinal view of soil microbial response to non-growing season conditions. Geochemical changes from flow-through leachate and amplicon sequencing of 16S and ITS rRNA genes were used to assess community response. Despite nitrification observed in fertilized columns, there were no significant microbial diversity, core community, or nitrogen cycling population trends in response to nutrient stress. FTC impacts were observable as an increase in alpha diversity during FTC. Community compositions shifted across a longer time frame than individual FTC, with bulk changes to the community in each phase of the experiment. My results demonstrate microbial community composition remains relatively stable for archaea, bacteria, and fungi through a non-growing season, independent of nutrient availability. This observation contrasts canonical thinking that FTC have significant and prolonged effects on microbial communities. In contrast to permafrost and other soils experiencing rare FTC, in temperate agricultural soils regularly experiencing such perturbations, the response to freeze-thaw and fertilizer stress may be muted by a more resilient community or be controlled at the level of gene expression rather than population turn-over. These results clarify the impacts of

winter FTC on fertilizer consumption, with implications for agricultural best practices and modeling of biogeochemical cycling in agroecosystems.

Acknowledgements

I am deeply indebted to all those that made this work possible including funding agencies, academic societies, collaborators, mentors, friends, and family. Throughout this research, I was primarily funded by an Ontario Graduate scholarship, the *rare* Charitable Research Reserve Ages Foundation Fellowship, and funding from my supervisor, Dr. Laura Hug. The research was primarily funded by the Canada Research Chair program in Environmental Microbiology and the winter Soil Processes in Transition project within the Global Water Futures program funded by the Canada First Research Excellence Fund.

I would like to give enormous thanks to my supervisor, Dr. Laura Hug, for her continued support and patience throughout my degree. Laura provided the necessary structure and atmosphere to allow intellectual independence as a scientist. She has allowed me ample opportunity to and flexibility within my degree in conferences, workshops, and employment. Lastly and most importantly, her empathy during the pandemic and prioritizing the physical and mental health of those in her lab above all.

I thank all those in the Hug Lab and Ecohydrology Research Group during my tenure, especially Konrad Krogstad who worked with my side by side on this work, literally sleeves rolled up arms deep in dirt, who always offered levity despite often messy dreary outings. I thank my committee members, Dr. Fereidoun Rezanezhad and Dr. Trevor Charles, for their continued support and useful feedback throughout all these years.

Lastly, I thank my friends and family for their continued support along this long journey. Special mention to my partner, Celine, who was always by my side.

Table of Contents

List of Figures

List of Abbreviations

16S	16S ribosomal RNA gene
amoA	ammonium monooxygenase
ANOSIM	analysis of similarities
ANOVA	analysis of variance
ASV	amplicon sequence variant
CCA	constrained correspondence analysis
Cl^-	chlorine
DC	dissolved inorganic carbon
DNA	deoxyribonucleic acid
EC number	enzyme commission number
Faith's PD	Faith's phylogenetic diversity
FTC	freeze-thaw cycles
hao	hydroxylamine oxideoreductase
ITS	internal transcribed spacer
nar	nitrate reductase
NCBI	National Centre for Biotechnology Information
NH_3	ammonia
NH_4^+	ammonium
nir	nitrite reductase
NMDS	non-metric multi-dimensional scaling
NO_2^-	nitrite

NO_3^-	nitrate
nor	nitric oxide reductase
nosZ	nitrous oxide reductase
nxr	nitrite reductase
OTU	operational taxonomic unit
PCoA	principal coordinate analysis
PCR	Polymerase Chain Reaction
PICRUSt2	phylogenetic investigation of communities by reconstruction of unobserved states 2
RNA	ribonucleic acid
rRNA	ribosomal ribonucleic acid
SOM	soil organic matter
TN	total nitrogen
TukeyHSD	Tukey's honestly significant difference (i.e., Tukey's test)
ureC	urease

Chapter 1 Introduction

1.1 Soil Microbes in the Non-Growing Seasons

It was commonly assumed the soil microbiome throughout winter remained inactive or in a state equivalent to hibernation. Early research identified large surges of microbial activity expressed as respiration, soil organic matter decomposition, and nitrogen mineralization after winter thaws (Gasser, 1958; Soulides and Allison, 1961; Mack, 1963). These studies suggest that the initial freeze results in a substantial cell lysis event, reducing the microbial biomass by up to 50% and enriching the soil by a 10-40-fold increase of sugars and amino acids – labile substrates that are consumed come the thaw (Ivarson and Sowden; Soulides and Allison, 1961). More recently, the notion of hibernation until the thaw was contested, as microbial respiration and denitrification has been detected below 0 °C in frozen soil, based on production of CO_2 and N_2O gases (Burton and Beauchamp, 1994; Clein and Schimel, 1995; Rivkina et al., 2000). Despite the majority of microbial activity being limited to post-thaw, greenhouse gas emissions throughout the winter transition are of a magnitude to contribute significantly to annual fluxes. Microbial activity in the winter season remains understudied, but it has gained recent attention due to implications for climate change, biogeochemical cycling, and agricultural management (Hayashi, 2014). Understanding the winter microbial activity and how it is controlled by temperature and snow cover is thus critical for climate change modeling.

Climate change will result in warmer winter temperatures, leading to a loss of insulating snowpack and thus colder temperatures for the active layer of soil. From this, the active soil layer will experience an increased number of freeze-thaw cycles (FTC) (Brown and DeGaetano, 2011). Approximately half of the landmass in the Northern hemisphere experiences seasonal freezing. A significant fraction of the world's total soil organic matter (SOM) is sequestered in

the permafrost of this region, which is at high risk for melting and decomposition (Zhang et al., 2003; Schuur et al., 2015). As many of the processes contributing to SOM decomposition are microbial, understanding the role and changing nature of microbial activity through the winter transition is an acknowledged need.

For studying winter soil processes, an individual freeze-thaw cycle acts as a blueprint for the full winter transition, where each freeze-thaw cycle follows approximately the same pattern of microbial activity. Ultimately, the entirety of the non-growing season can be viewed as a series of FTC of varying frequency and length (duration of freeze and thaw). Broadly, microbial activity is stunted as temperatures decrease, and the freeze leads to cell lysis (Graham et al., 2012). If an ice front is formed at the top of the soil, it creates a diffusion barrier allowing for generation of temporary anaerobic conditions (Yanai and Toyota, 2005). Respiration and denitrification from the soil, while diminished, continue even during the freeze (Clein and Schimel, 1995). Upon thawing, the soil releases trapped gases as the diffusion barrier melts and unfrozen water becomes accessible (Rivkina et al., 2000). The flushing event from melting is accompanied by oxygen and labile nutrients from lysed cells, roots, and disrupted soil aggregates. This influx of nutrients aids in recovery of heterotrophic microbial populations (Hayashi, 2014). Denitrification continues briefly after flushing, as the necessary gene products are still expressed, but quickly stops after the return of oxygen (Teepe et al., 2001). The winter transition, when viewed as a series of FTC, is a system of diminishing returns, as the magnitude of respiration (measured via gas flux) decreases with each cycle (Hayashi, 2014).

To properly characterize microbial activity from winter soils, multiple metrics have been employed including measuring microbial biomass, metabolism, gene product expression, and community composition (Nikrad et al., 2016). A combination of metrics allows for a holistic

view of microbial activity, as, at any given moment, 95% of microbial biomass in soil may be dormant with the bulk of the observed metabolism being carried out by a minority of the total community (Kuzyakov and Blagodatskaya, 2015). During the dynamic temperature shifts of a freeze-thaw cycle, different populations within the community will become active depending on a host of environmental variables including the degree of snow cover, access to liquid water, temperature, and nutrient availability (Figure 1.1, from Nikrad et al., 2016). Each microbial population (and their activities) will respond to these changing variables within the larger system of winter soil processes, such as the changing physical, hydrological, and geochemical properties of soils (Figure 1.2, from Hayashi, 2014). Thus both the changing environmental variables that impact microbes in soil, and how microbes react to those changes must be understood to characterize the soil microbiome.

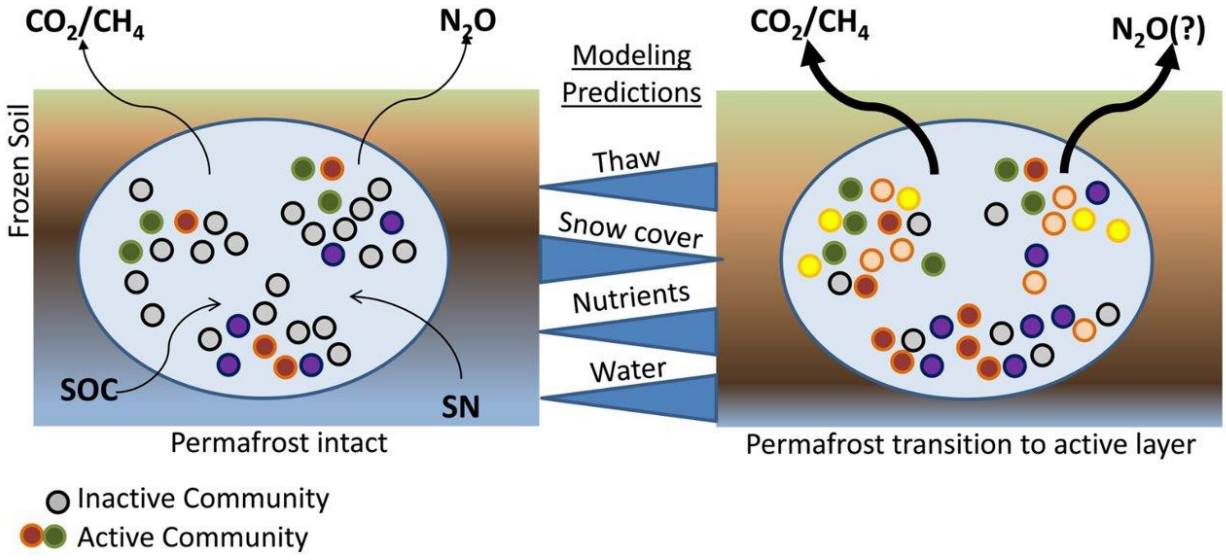

Figure 1.1: Dynamic microbial activity is determined by environmental variables, thus both the changing environmental conditions and the microbial responses to these changes must be modeled. Left: frozen permafrost and baseline microbial activities. Right: shift in microbial community activity and community composition under thaw conditions. Middle: factors to be modeled to predict the observed shifts. Figure by Nikrad *et al*. (2016).

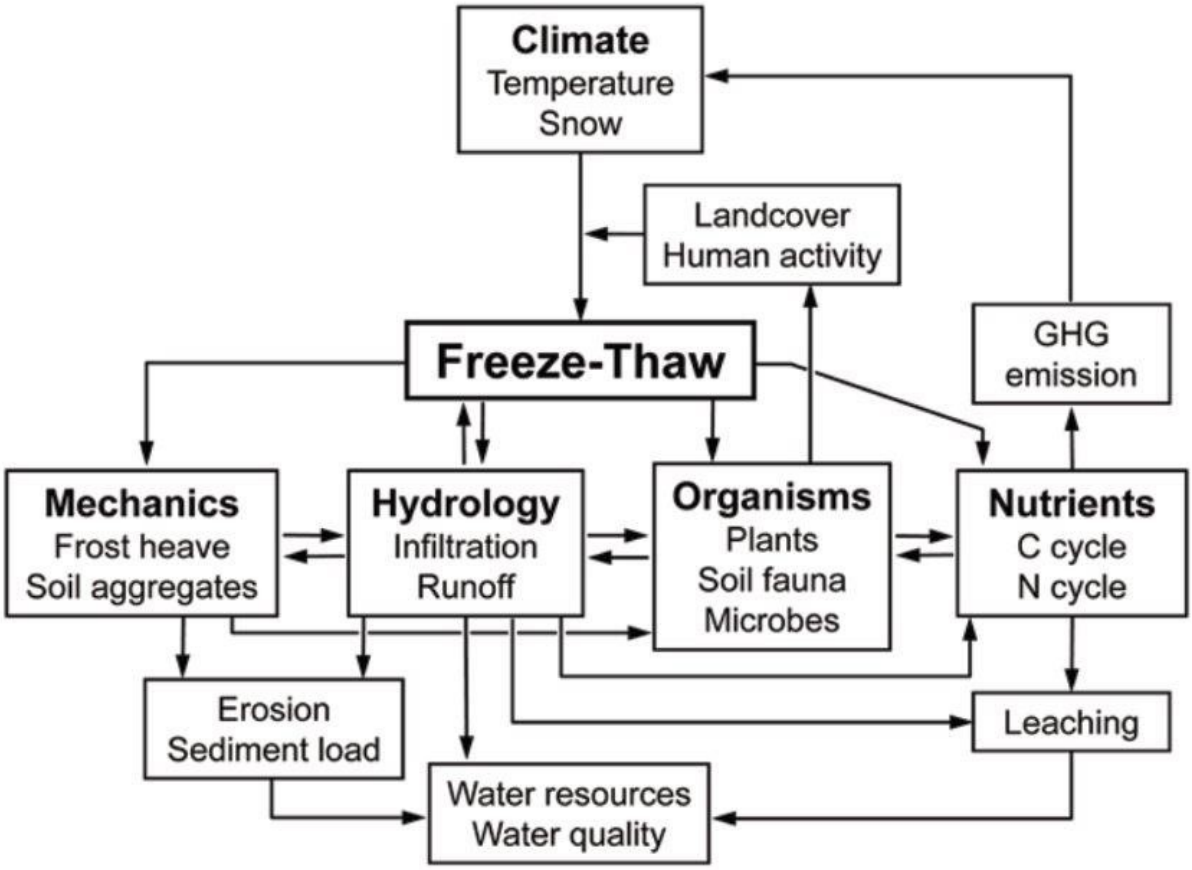

Figure 1.2: Feedback of soil freeze-thaw processes at the macro level: environmental variables impact microbial growth and community composition. Figure by Hayashi (2014).

Conflicting experiments have led to inconsistent results, as some studies have noted decreases, increases, or overall conservation of microbial biomass throughout the winter transition (Pesaro et al., 2003; Schadt et al., 2003; Yanai and Toyota, 2005). These contradictory results are not necessarily a failure of reproducibility but may instead be a result of different environmental factors impacting cell lysis and cell growth.

1.2 Factors Influencing Impacts of Freeze-Thaw Cycles

1.2.1 Snowpack Insulation

Variations in microbial biomass can be explained by the degree to which the soil was insulated from the air temperature, under either imposed temperature regimes or *in situ* experiments (Henry, 2007). In work by Brooks et al. (1998) and Schadt et al. (2003), an increase in biomass was not reported for freeze-thaw cycling, except for in undisturbed soils with an intact snowpack and ready supply of carbon. In this instance, heterotrophic growth was favourable under the snowpack. Upon snowmelt and throughout the summer, the microbial biomass sharply declined. In contrast, in the absence of insulation or with intermittent snow cover, the soil is exposed to freezing air temperatures and either a decline or conservation in biomass is observed (Pesaro et al., 2003; Yanai and Toyota, 2005).

1.2.2 Properties of Unfrozen Water

Soil is characterized by the formation of micro-sites depending on the topography of the pore network, allowing for heterogeneous niche areas of microbial growth (Yanai and Toyota, 2005). These sites are formed by the unfrozen water in soils under frozen conditions. Due to the equilibrium conditions of the water phase change, the amount of unfrozen water diminishes quickly with small changes below 0 °C. The remaining water is present as films on soil particles and small pores (Hayashi, 2014). However, the volume of bioavailable water will depend on the freeze-thaw parameters of the experiment. Due to the hysteresis-like behavior of rapid freeze/thaws, water content in soils depends on the rate of FTC, with faster freezing leading to higher water content (Watanabe and Osada, 2017). The rate of FTC similarly impacts the formation of ice, where rapid shifts in temperature lead to less damaging intracellular amorphous ice formation (in contrast to ice crystals) and gradual regimes lead to more damaging extracellular ice formation. Extracellular ice damages microbial populations by increasing solute

concentrations and cell dehydration, and causing membrane damage (Walker et al., 2006). Additionally, freezing may change the pH of the microbial microenvironment, where pH is generally considered the most significant driving factor influencing community composition (Fierer, 2017).

Microbes are limited by their reliance on diffusion for access to nutrients and for waste removal, both of which are determined by the volume of unfrozen water in winter soils (Yanai and Toyota, 2005). Rivkina et al. (2000) determined the importance of unfrozen water content on microbial activity in winter conditions. The study observed metabolic activity in permafrost soils at temperatures as low as -20 °C through incorporation of ^{14}C-labeled sodium acetate. Incubation of soils across a range of temperatures showed different growth rates but also differences in the magnitudes of stationary phase communities, meaning that more aggregate growth was possible for higher temperatures of soil. Stationary phase typically implies depletion of nutrients, however since the researchers provided a steady nutrient supply, it was determined that the unfrozen water content was the limiting factor (Rivkina et al., 2000).

1.2.3 Microbial Temperature Sensitivity

A reduction or change to microbial biomass and diversity can be partially characterized by the ratio of bacterial to fungal biomass. Several studies have identified that the winter transition favors the growth of fungal taxa (Schadt et al., 2003; Henry, 2007). It has also been observed that fungi may be more temperature resistant than bacteria, as laboratory induced FTC by Sharma et al. (2006) revealed total microbial biomass was conserved while the fungal population remained more consistent than the bacterial populations based on rRNA fingerprinting. At the time, it was suggested either temperature resistance, limited initial diversity, or dominance of bacteria could explain reduced fungal community shifts. Conversely, Feng et al. (2007) utilized

phospholipid fatty acid assays to measure bacterial and fungal biomass separately, demonstrating that over 10 FTCs, the fungal biomass was significantly reduced while bacterial biomass was conserved. Inconsistencies across these experiments may be attributed to methodological differences, as suggested by Henry (2007), most notably the differences in thaw times. Sharma et al. (2006) observed that it took 9 days of thaw for community compositional differences to become apparent.

Initial FTC may be more disruptive to bacterial communities due to temperature sensitivity, but bacterial biomass is capable of rapid recovery due to flexible metabolisms and shifts in the community composition. In contrast, fungal populations are more suited to colder temperatures and thus survive when insulated, as seen in work by Schadt et al. (2003), however fungi are more sensitive to freeze-thaw stresses. Aanderud et al. (2013) measured the fungi to bacteria biomass ratios with *in situ* experiments at different soil latitudes (with corresponding different soil freeze depths). They observed increases in fungi to bacteria ratios in soils with freezing limited to just the active layer. Thus, without continued exposure to freeze-thaw stress, increased fungal tolerance was observed. The authors attributed this to extended hyphae (filamentous growth) allowing fungi access to nutrients and water from deeper soils. This phenomenon has also been observed for bacterial strains, where Walker et al., (2006) reported that it was not the absolute temperature but FT cycling that was more disruptive to cell counts and diversity. Further, Walker et al. reported that, for some strains, only the initial freeze-thaw was deleterious to biomass, with subsequent FTCs having less of an impact, implying potential community/population adaption, or cell death of all non-adapted to freeze-thaw stress (Walker et al., 2006). Microbes, if given sufficient time, may employ adaptive strategies including adjusting membrane fluidity,

production of anti-freeze proteins, and use of cold-active enzymes (Walker et al., 2006; Hall et al., 2010).

1.2.4 Substrate Availability

Substrate availability limits microbial activity and growth, while the community composition determines the affinity for SOM degradation and substrate selectivity. Herrmann and Witter (2002) established that the influx of labile carbon produced by FTCs was from microbial lysis and disruption of soil aggregates, at 65% and 35% respectively. Without additional inputs, this limited supply of nutrients diminishes with subsequent FTCs, depleting microbial access to carbon and nitrogen (Herrmann and Witter, 2002).

Feng et al. (2007) attempted to identify the source of the CO_2 flux by amending soil with grass powder (characterized largely as labile carbon) and alkali lignin (recalcitrant carbon) while extracting free lipids, bound lipids, and lignin-derived phenols from the soil after exposure to FTC. Microbial biomass nearly doubled in the grass powder amendment, due to enrichment of free lipids. However, actual CO_2 emission did not increase proportionally to the quantity of free lipid that was added, and in all instances, free lipid was consumed quickly after several FTC, while recalcitrant forms of carbon remained stable and were not consumed. This suggested that free lipid freed from soil aggregates masked the initial consumption of free lipids (as levels were stable for the first few FTC). These results matched the conventional belief that heterotrophic respiration favours labile carbon and microbes discriminate based on SOM quality. Availability of such labile sources becomes difficult with depth and as such taxa typically associated with recalcitrant carbon consumption are detected at lower depths in mineral soils (Deng et al., 2015). Deeper soils are typically limited in labile carbon and thus deeper soil communities reflect

metabolisms capable of digesting more recalcitrant carbon sources (Taş et al., 2014; Deng et al., 2015).

Similarly fertilizer, which is typically added either late fall, mid-winter, or early-spring to provide nitrogen and phosphorus to depleted soils for crops, will change the nutrient availability for microbes (Romero et al., 2017). Concerns of fertilizer efficacy and when it should be applied have arisen as run-off, immobilization, denitrification, or NH_3 volatility all reduce fertilizer potency, often considerably more so following fall applications (Chantigny et al., 2017; Romero et al., 2017). Some of this fertilizer loss can be attributed to continued microbial activity at winter temperatures in the soil. Animal slurry-style fertilizers introduced in the fall are matched by increased greenhouse gas flux during the non-growing season, as soil heterotrophs are readily equipped to utilize the labile carbon and nitrogen substrates within (Chantigny et al., 2017; Romero et al., 2017). Herzog et al. (2015) observed that microbial community shifts occur as a result of fertilizer addition throughout the non-growing season compared to soils without additions. The observed change largely consisted of changes to the active community, including the enrichment of genes encoding for cellular nitrogen uptake, nitrification, and denitrification pathways. In addition to conventional losses of fertilizer potency attributed to fall applications, the warming winter (due to increased frequency of FTC) may reduce fertilizer potency further as microbial activity increases with the rising temperatures and more frequent thaw events. This has implications for agricultural best management practices with potential modifications to how fertilizer should be applied to align with the 4R Nutrient Stewardship principes (i.e., right source, right rate, right time, right place; Johnston and Bruulsema, 2014).

1.3 Microbial Activity During Freeze-Thaw Cycles

Microbial activity during freeze-thaw cycles is decoupled from aggregate biomass, as the activity of a single cell is dynamic and not constant throughout FTC (Feng et al., 2007). Total greenhouse gas emissions from carbon respiration and denitrification in this time period contribute significantly to annual GHG budgets (Hayashi, 2014).

1.3.1 Respiration

Heterotrophic respiration producing CO_2 can be observed even while soils are frozen, but significantly increases during thaw events (Du et al., 2013). Freeze-thaw cycling creates flush events of labile nutrients that provide the carbon for respiration, but with diminishing returns during subsequent FTC (Graham et al., 2012). As respiration continues throughout the growing season, winter soil CO_2 emissions contribute approximately 5% of annual CO_2 soil emissions (Matzner and Borken, 2008).

Heterotrophic respiration has been well characterized as connected to newly available nutrients from cell death during FTC (Schmidt and Lipson, 2004; Lipson et al., 2009). Over the course of the winter transition, soil can experience a slow accumulation of microbial biomass, potentially as a result of extended fungal hyphae growth, increased carbon use efficiency at low temperatures, and the release of labile carbon by roots in the late winter (Schadt et al., 2003; Lipson et al., 2009; Tucker et al., 2014). Through minimal photosynthesis at low temperatures the rhizosphere (soil environment adjacent to plant root networks) is still capable of activity as nutrients and carbon are still being provided (Larsen et al., 2007; Tucker et al., 2014). Further studies revealed that across the winter transition the total carbon respiration was approximately 35% from the rhizosphere and 65% from the heterotrophs (Tucker et al., 2014). This is an important consideration, as heterotrophic respiration contributes to carbon loss as previously-

sequestered CO_2 escapes into the atmosphere, whereas rhizospheric respiration merely returns carbon that was previously fixed by the plant back to the atmosphere (Tucker et al., 2014).

1.3.2 Denitrification

Denitrification in the non-growing season contributes significantly to annual N_2O budgets, estimated at up to 50% of annual release, but over a brief period of time (Hayashi, 2014). Anaerobic pathways like denitrification are favoured once ice forms a diffusion barrier, maintaining a minimal oxygen environment as well as access to labile carbon provided by FTC (Nikrad et al., 2016). It was initially thought that trapped gas may contribute to a significant portion of the observed N_2O. Emission experiments involving sterilized frozen soils by Röver et al. (1998) showed no evidence of denitrification nor N_2O emission, which clarified the N_2O is a direct result of currently-active microbial processes. Sharma et al. (2006) further demonstrated that the activity of denitrification was decoupled from biomass, as biomass was largely conserved throughout their experiment and community compositional changes only become significant several days after the peak of N_2O release.

1.4 Microbial Community Membership

Current research into winter transitions and microbial activity has leveraged high-throughput amplicon sequencing to explore the effects of FTC and the winter transition from total community diversity to specific taxa scales. Ultimately, microbiome composition differs with soil type and the nature of the study, making direct comparisons difficult. Thus, only the relative changes, the corresponding drivers (soil properties), and main inferences of that change are highlighted in the examples below.

Han et al. (2018b) observed vertical variation in microbial diversity of black soil in laboratory-controlled freeze-thaw cycle experiments. Among bacteria and archaea, the dominant shift was

from Proteobacteria to Actinobacteria with a richness decline and conservation of diversity including Actinobacteria, Thaumarchaeota, and Tectomicrobia dramatically increasing in relative abundance while Gemmatimonadetes, Verrucomicrobia, and Saccharibacteria sharply declined. Among fungi, only the Ascomycota showed significant changes, while overall diversity and richness were unaffected. Moisture, electrical conductivity, and pH were found to be the dominant drivers of these shifts.

Müller et al. (2018) used an *in situ* experiment to measure microbial community composition in permafrost soil in the active layer, permafrost layer, and transition zone in a 2 m soil core encompassing all layers. Along the depth gradient, the dominant phyla of Acidobacteria, Actinobacteria, Proteobacteria, and Verrucomicrobia in the active layer were replaced by a community dominated by Actinobacteriota and Bacteroidetes in the permafrost layer. The community composition changed dramatically across just 3 cm of soil. Thus, the presence of thaw events (as in the active layer) is a significant determinant of community change.

Ren et al. (2018) collected soil from a seasonally frozen marsh before the first freeze-thaw cycle and after the last freeze-thaw cycle in the autumn and spring seasons. Following the autumn freeze-thaw cycle, bacterial abundances remained the same, but community composition changed as Acidobacteria and Gammaproteobacteria increased in the thaw while Firmicutes were more dominant while the soil was frozen. No significant changes were found between spring freeze and thaw. This implied the selection event of the winter transition changes occurred early in the season, potentially immunizing later communities against FTC.

Žifčáková et al. (2016) examined the diversity (DNA) and metatranscriptomes (RNA) of the coniferous forest soil and litter microbial communities in the summer and late winter. Changes in relative abundance of DNA for bacterial and fungal groups was largely limited to a few taxa such

as Actinobacteria (increasing), while significant differences were more strongly correlated to differing populations in litter matter compared to soil, rather than seasonal. For seasonal changes, fungal activity (transcription and diversity dominated by Basidiomycota and Ascomycota) decreased significantly in the winter with relatively constant biomass. The driver for this was assessed as the difference in plant photosynthesis over seasons, as the dominant fungi were ectomycorrhizal fungi, associated with plant roots.

Overall Actinobacteria seem to consistently demonstrate higher immunity to freeze-thaw and winter-related stressors. Unfortunately, most previous studies have been limited in temporal resolution to the changes in microbial composition over the whole winter transition, with few or no intermediate time points, and only over the course of a single annual cycle.

1.5 Study Objectives

In this study, we examined the impact of FTC in combination with fertilizer treatments on microbial communities in agricultural soil using a temperature-controlled column experiment. We monitored geochemical changes and microbial community diversity over a 60-days experiment simulating a compressed non-growing season that is typically 180 days (winter plus portions of the shoulder seasons). The impacts of repeated freeze-thaw cycling and nutrient stress on bacterial, archaeal, and fungal community membership were determined, providing a deeply sampled longitudinal view of soil microbial response to winter conditions over the course of the non-growing season.

Chapter 2 Materials and Methods

2.1 Soil Collection, Preparation, and Characterization

Soil was collected from the Southern agricultural field at the *rare* Charitable Research Reserve located in Cambridge, Canada (latitude 43°22′39.80″N; longitude 80°22′07.28″W). Soil samples were collected in mid-October 2018 before the first snowfall or any freezing of the soil. The surface vegetation (grass) was removed and the top-soil horizons (A-horizon: 0–18 cm depth) were collected. The Southern field location has been historically cultivated but had been fallow for the prior 2 years and had not been fertilized prior to soil collection. Once collected, the soil was sieved to retain only 1–2 mm soil aggregates and then homogenized. Soil was kept at 10°C for ∼1 week prior to the column experiment. The soil particle size distributions were determined via the pipette method by the Agriculture and Food Laboratory at the University of Guelph (Gee and Bauder, 1986). It was characterized as a loamy soil with 52%, 32%, and 16% of silt, sand, and clay, respectively. Soil total porosity and bulk density were determined gravimetrically from the saturated mass, the oven-dried (105°C for 24 h) mass and the original volume of the sample, following the method of Boelter (1972). The pH was 7.2 with total porosity and bulk density as 1.22 g cm^{-1} and 0.54, respectively.

2.2 Soil Column Experimental Setup

The freeze-thaw soil column experiment was conducted using four columns (Figure 2.1). Each column was composed of hard acrylic, with an inner diameter of 7.5 cm and length of 60 cm (Soil Measurement Systems, LLC, United States). Approximately 2.5 kg of sieved and homogenized soil were packed evenly between the four columns, to a column height of 50 cm. Soil homogenization, while disrupting the native soil structure, mimics the practice of tillage in agricultural soils. Duplicate columns were prepared for two experimental treatments: unfertilized

(columns Unfertilized 1 and 2) and fertilized (columns Fertilized 1 and 2). All four columns were placed in an environmental chamber incubator (Percival I-41NL XC9) and subjected to a simulated winter transition temperature regime. Columns were equipped with a 150-W band-heater (120V, 2 W/inch^2, custom produced by Gordo Sales Inc.) surrounding the lower 40 cm of each column that maintained the temperature at 8°C in the lower portion of the soil to mimic the subsurface temperature gradient in southern Ontario's soil (Funk et al., 1980; Conant, 2004; Zhang, 2005). Time-series temperature data was recorded every 15 min during the experiment by temperature sensors (PT-100, DaqLink Fourier Systems Ltd., #DBSA720) installed in one of the soil columns (Fertilized 1) at depths of +2.5, −3.5, −7, -−15.5, and −33 cm relative to the soil surface, with one additional sensor in the chamber to monitor air temperature. Soil columns were designed to allow sampling of the leachates, collected from the bottom of the columns, and soil samples via a series of side ports. Prior to the start of the experimental conditions, the columns were saturated with artificial pore water (composition below) and then allowed to drain. For a more detailed explanation of the soil column setup, see Krogstad et al. (2022).

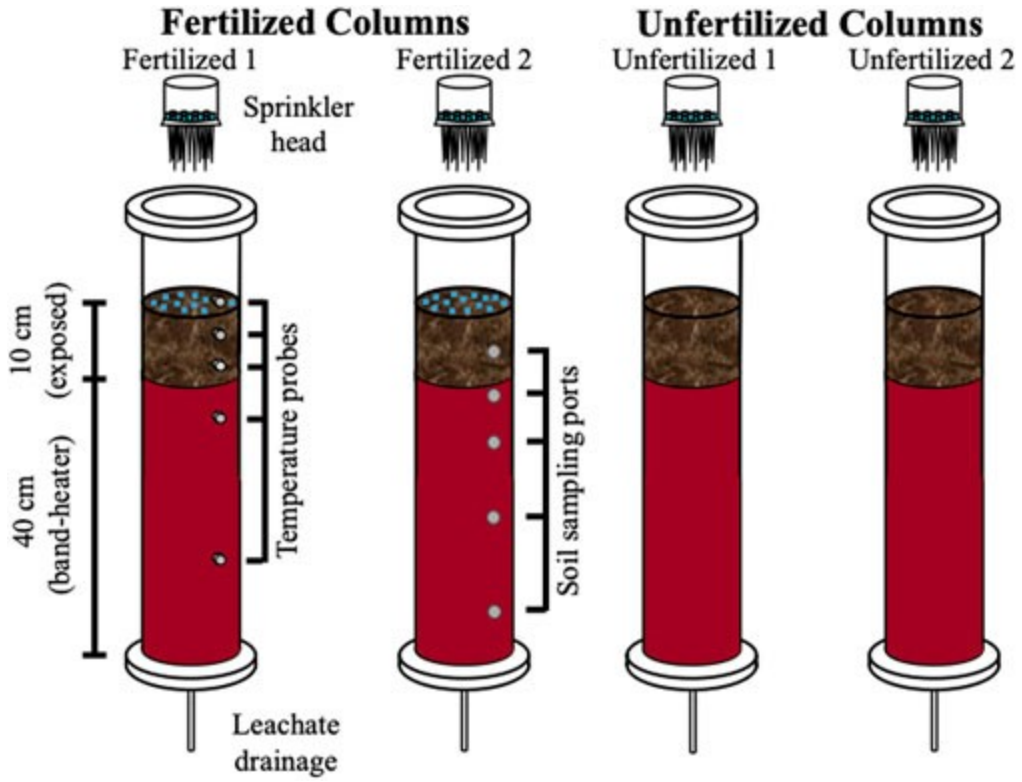

Figure 2.1: Schematic diagram of soil columns. Four columns were packed with agricultural soil, with two columns amended with fertilizer. A sprinkler head allowed for application of precipitation which is then collected as leachate after flow-through. Temperature probes, at depths of +2.5, −3.5, −7.0, −15.5, and −33.0 relative to the soil surface were used to track the simulated temperature gradient across depth created by the environmental chamber and insulating band heater (instrumented and indicated on Fertilized 1 column, not present in other three columns). Ports at depths of −5, −11, −18, and −38 cm were used to sample for soil (indicated on Fertilizer 2 column but ports were present on all four columns).

2.3 Fertilizer Treatments

The fertilizer selected was Miracle Gro Ultra Bloom water soluble Plant Food. It is a 15-30-15 N-P-K fertilizer with primary constituents by mass of 15% total nitrogen (5.8% ammonia chloride and 9.2% urea), 30% phosphate (P2O5), and 15% soluble potash (K2O). Fertilized columns were amended using 1 g of fertilizer sprinkled uniformly on to the surface of the soil. This was necessary for uniform distribution over the 45.6 cm2 surface area of the columns. In

normal field conditions (at rare) the fertilizer is applied at a rate of 8.6 g m−2 (190 lbs ha−1) and thus this experiment utilized a 20-fold increase compared to the agricultural rate.

2.4 Simulated Non-Growing Season Climate Conditions

All four columns were exposed to a simulated climate model based on the average of 3 years of locally monitored air temperature and precipitation (rain and snow) over winter and shoulder seasons in Southern Ontario (CAPMoN, 2018). Diurnal highs and lows were simulated by fluctuating 8–10°C, oscillating every 12 h, with the chamber incubator taking approximately 2 h to adjust to temperature. An artificial mid-winter premature thaw was added to simulate expected temperature increase from winter climate warming. The climate model was then condensed into a 56-days experiment, where each simulated month was represented by 9 days (Figure 2.2). Precipitation was measured by mm of precipitation over a full non-growing season and adjusted to fit the shortened timeframe of the climate model and surface area of the soil columns.

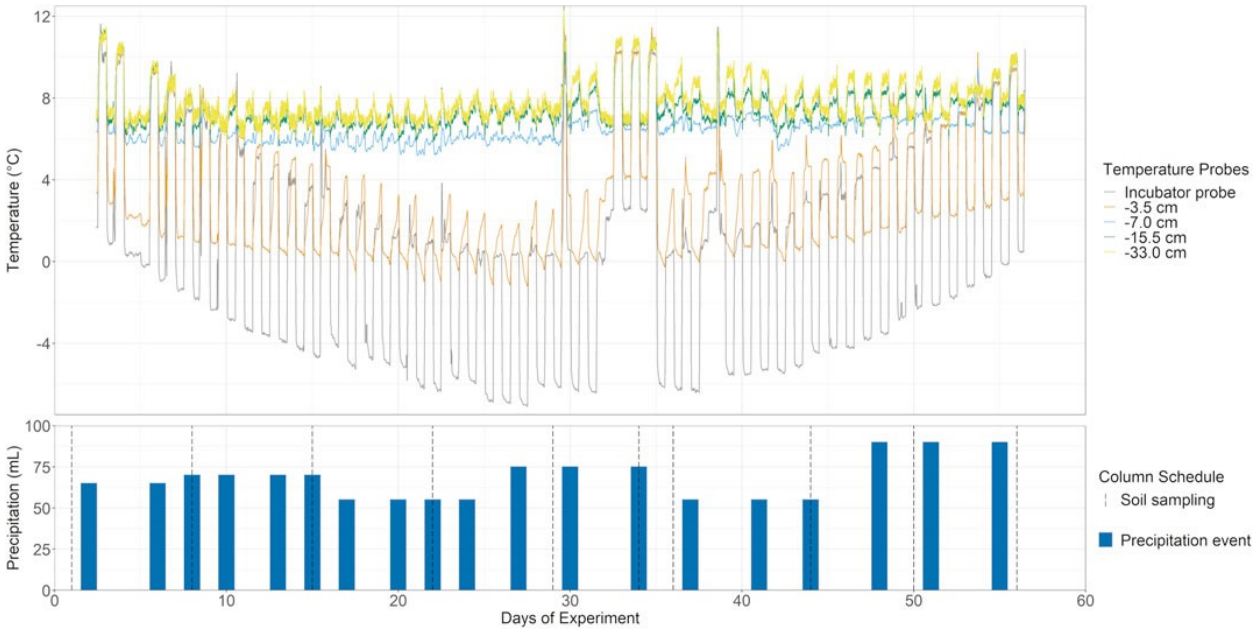

Figure 2.2: Temperature and simulated climate model. Top: Five temperature probes including ambient incubator air and various soil depths were used to monitor the simulated non-growing

season, with additional premature mid-winter thaw, in the soil columns over 56 days. Insulation from the band-heater prevents FTC in all but the shallowest measured depth at −3.5 cm. Bottom: Precipitation based on simulated climate data was added over the course of the experiment via sprinkler head and collected as leachate periodically. Soil sampling occurred approximately once a week, except for a higher resolution over the premature winter thaw (ten sampling points, grey dotted lines).

2.5 Artificial Rainwater and Sampling

Precipitation for the soil columns was conducted using a synthetic pore water equivalent with milli-Q water as a base and the following additions: 22.6 µM SO_4^{2-}, 42.7 µM NO_3^-, 5.52 µM Cl^-, 44.92 µM NH_4^+, 4.34 µM Na^+, 12.12 µM Ca^{2+}, 3.41 µM Mg^{2+}, 1.26 µM K^+, adjusted to a pH of 5.15. Artificial rainwater was added via a sprinkler head, with 55–90 ml of artificial rainwater amended 2-3 times per week (Figure 2.2). The flow-through leachate samples were collected from the four columns periodically over the experiment (the leachates were typically available 1 day after rainwater application; Figure 2.2). The soil ports were installed at multiple depths from the surface soil and sampled at -5, -11, -18, and -38 cm. All soil ports were sampled approximately weekly with 10 sampling points over the course of the 56 days of the experiment (Figure 2.2, dotted lines).

2.6 Geochemical Analysis of Leachate

The leachate samples were analyzed for pH and electrical conductivity using LAQUtwin meters (model Horiba B-213). Leachate was filtered through 0.2 µm Thermo Scientific Polysulfone membrane filters and then further processed for major anions including chloride (Cl^-), nitrite (NO_2^-), and nitrate (NO_3^-) using ion chromatography on the IC Dionex ICS-5000 (with capillary IonPac® AS18 column; ± 3.0% error and ±1.6% precision. Calibration for each analyte was performed with a multiple point linear regression using Dionex Chromeleon 7.0 chromatography

software generated with external standards tested in triplicate (ranging from 0.5 to 30 mg L^{-1}) from diluted certified standards.

2.7 DNA Extraction and Sequencing

Soil samples were collected from all four columns at each of four depths (−5, −11, −18, and −38 cm) of about 0.5 g of soil per depth, at ten sampling timepoints (shown in Figure 2.2) for a total of 160 samples. Total environmental DNA was extracted from 0.25 g of each soil sample using the QIAGEN DNeasy Powersoil Kit as per the manufacturer's protocol (discontinued; Ref# 12888-100). Amplicon sequencing of marker genes was performed to characterize the bacterial, archaeal, and fungal populations in the soil. For bacteria and archaea, the V4 region of the 16S rRNA gene was amplified by PCR using the 515F and 806R primers, and for fungi the inter-transgenic space 1 (ITS1) region was targeted using the BITS and B58S3 primers (Bokulich and Mills, 2013; Walters et al., 2015). All 160 soil samples were used in the 16S rRNA survey but only 7 of 10 time-points were chosen for ITS rRNA sequencing, for a total of 112 samples in the ITS survey. PCR amplification and paired-end Illumina sequencing were performed by MetagenomBio (ON, Canada), with sequencing conducted on an Illumina MiSeq generating 2 × 150 bp reads (Illumina, United States).

2.8 Bioinformatic Analysis

Microbiome analyses were first processed using the QIIME2 2020.2 pipeline (Bolyen et al., 2019). Raw sequence data imported as paired-end demultiplexed reads in the Casava format were first truncated to remove primers from the read ends via the plugin cutadapt version 3.3 (Martin, 2011). Reads were then quality filtered using the q2-demux plugin, and subsequently denoised with DADA2 using q2-dada2 (Callahan et al., 2016) generating amplicon sequence variants (ASVs). Taxonomic classification was performed on ASVs via q2-feature-classifier

(Bokulich et al., 2018) classify-sklearn naïve Bayes taxonomy classifier using the SILVA 138 99% operational taxonomic units (OTUs) reference sequences for bacteria and archaea (Quast et al., 2013), and the UNITE 8.2 99% dynamic OTUs reference sequences for fungal reads (Nilsson et al., 2019).

QIIME2 core metrics were used to generate values for 16S and ITS rRNA alpha diversity scores of observed ASVs, Shannon score, and Faith's phylogenetic distance (PD). RStudio, version 1.4 with *R* version 4.1 (RStudio Team, 2020), was used to generate beta diversity scores for Jaccard, Bray-Curtis, and Unifrac (weighted and unweighted) distances of the raw ASV abundances for principal coordinates analysis (PCoA) using the qiime2R, phyloseq, vegan, and dplyr packages (McMurdie and Holmes, 2013; Bisanz, 2018; Oksanen et al., 2019; Wickham et al., 2021). Bray-Curtis distances of ASV relative abundance were used for non-metric multi-dimensional scaling (NMDS), and constrained correspondence analysis (CCA) to visualize the contribution of environmental and categorical variables to sample similarity using the "envfit" function from the vegan package. All visualizations were generated in *R* using the ggplot2, and ggpubr packages (Wickham, 2016; Kassambara, 2020). All community and diversity assessments were made using ASVs rather than clustered OTUs.

Core community selection was performed by ranking ASVs based on temporal occupancy (persistence) first and then by their contribution to Bray-Curtis beta diversity as described by Shade and Stopnisek (Shade and Stopnisek, 2019) using the *R* package 'dplyr'. All samples were used to assess core members. Index ranks were determined by weighing the sum of both time-specific occupancy and time-point replication consistency such that persistent ASVs are prioritized. Bray-Curtis similarity was then calculated for the whole dataset but then individually for each top-ranked taxa. Individual ASV contribution is determined on its percentage of the

total beta diversity. Index ranks are included as core members until a threshold of diminishing contribution to beta diversity is achieved by the last ranked ASV having to exceed a 2% increase in from the last cumulative Bray-Curtis similarity of the previously ranked ASV. All ranks up to the last ASV with a 2% increase to BC similarity were then added as core members. The list of selected core ASVs was then used to filter the feature table of the entire dataset and plot the cumulative core list relative abundance across time and fertilizer treatment. This approach differed only from Shade and Stopnisek (2019) by virtue of using ASVs rather than 97% OTUs and explicit use of the percentage threshold rather than "elbow" method.

PICRUSt2 version 2.3.0-b (Douglas et al., 2020) was used to predict potential function for ASVs (from the QIIME2 output) based on similarity to known organisms with complete genomes. Putative nitrogen cycling ASVs were grouped together based on predicted potential nitrogen cycling enzymes via shared Enzyme Commission (EC) number. Nitrogen cycling enzymes included: urease (*ureC*; EC 3.5.1.5), ammonium monooxygenase (*amoA*; EC 1.4.99.39), hydroxylamine oxidoreductase (*hao*; EC 1.7.99.1), nitrite oxidoreductase (*nxr*; EC 1.7.1.15), nitrate reductase (*nar*; EC 1.7.99.4), nitrite reductase (*nir*; EC 1.7.2.1), nitric oxide reductase (*nor*; EC 1.7.2.5), and nitrous oxide reductase (*nosZ*; EC 1.7.2.4). Similar to the core community analysis, each specific EC-bearing community was assessed via changing relative abundance with time and across fertilizer treatment.

2.9 Statistical Analysis

Significant changes to the microbial community alpha diversity were evaluated first by ANOVA to determine significance by categorical variables of column, depth, fertilizer, and time (days of experiment) using the *R* package vegan. For significant variables, Tukey tests were used to identify specific significance within variables between groups using the "TukeyHSD" function

in *R*. To assess the variable of "time" with a parametric test, sampling dates were grouped to categories of "phase" including pre-FTC (days 1, 8, and 15), during FTC (days 22, 29, 34, 36, and 44), and post-FTC (days 50 and 56). Similarly, Tukey tests were used to identify significant differences for potential predicted nitrogen-cycling-enzyme-bearing and core communities between fertilized and unfertilized treatments, and between temporal phases. The degree and significance of differences in community compositions across sample types were evaluated in the canonical ordinations using the analysis of similarities (ANOSIM) test with Bray-Curtis distances of relative ASV abundances (Clarke, 1993) using the 'anosim' function in the vegan package.

2.10 Data Availability

The datasets presented in this study can be found in the NCBI SRA database (https://www.ncbi.nlm.nih.gov/) under accessions SRX14619372 - SRX14619626.

Chapter 3 Results

3.1 Simulated Climate Model and Geochemical Properties of Leachate

Soil columns experienced the entirety of the desired simulated climate model for 56 days. Insulation provided by the band creators worked to establish a temperature gradient across depth (Figure 2.2) with only freezing (recorded temperatures below 0°C) occurring at the top layer (3.5 cm depth probe). Frost heave was observed in all columns penetrating below the shallowest soil sampling depth of 5 cm (Figure 3.1), appearing after approximately 15 days into the experiment. Acidity measurements of column leachates observed a pH range of 6.5–8.5 among unfertilized, and 7.0 to 8.5 in fertilized columns. EC values ranged from 0.1 to 170 μS cm^{-1} for unfertilized, and 0.1 to 200 μS cm^{-1} for fertilized columns. Krogstad et al. (2022) calculated the residence time of the fertilizer through the columns as ~13.9 days, confirmed with elevated Cl^- tracer observed after 15 days from the fertilized columns' leachates. This increased until a maximum at 30 days during the midwinter thaw and declined until reaching equivalent levels to the unfertilized columns indicating clearance of fertilizer through the entirety of the column length over the experiment timeframe (Figure 3.2). NO_2^- levels were consistent and similar between unfertilized and fertilized columns pre- and post-FTC, but experienced a sharp decline to non-detectable levels in fertilized columns after 22 days, before recovering after 44 days. The NO_2^- decrease in fertilized columns coincided with a rising NO_3^- concentration, which continued to rise until the final day 59, reaching peaks of 150–160 mg L^{-1}. Within the unfertilized columns, NO_3^- concentrations remained minimal throughout.

Figure 3.1: Evidence of soil freezing in the top soil layer. An image taken of the Fertilized 1 column indicating visible frost heave of the top soil layer (approximately 5 cm) after subsequent freeze-thaw cycles as per the simulated climate model.

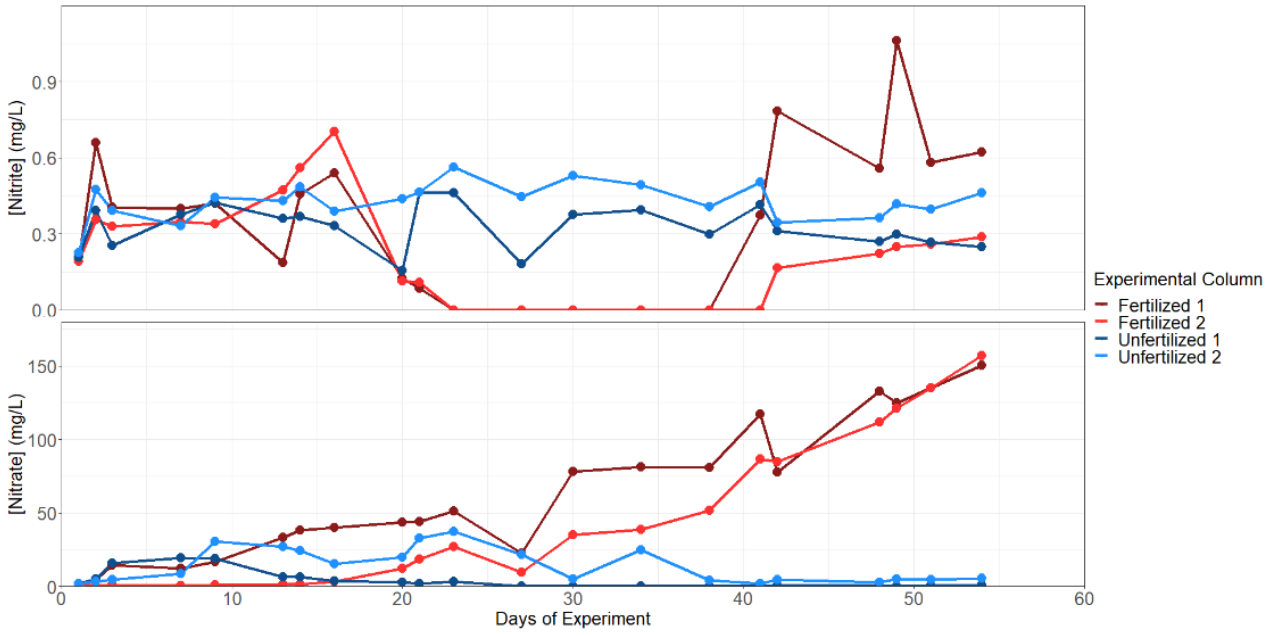

Figure 3.2: Measured nitrate and nitrite concentrations per soil column. Leachate flow-through from each soil column was collected post simulated precipitation and measured for nitrite (top)

and nitrate (bottom) via ion chromatography on the IC Dionex ICS-5000. Soil columns are differentiated by colour for fertilized (reds) and unfertilized (blues) and replicate number (each column's leachate plotted separately).

3.2 Sequencing Quality, Reads, and Major Taxa

For 16S rRNA amplicons, a total of 3,391,693 paired end reads were generated with an average read length of 253.25 nucleotides. The minimum library size was 4,348 merged reads, and a total of 7,390 ASVs were identified from all soil samples. For ITS rRNA amplicons, only 99 samples passed filtering to a minimum sequencing depth of 1,000 reads, leaving a 1,435,004 paired end reads with an average read length of 205.26 nucleotides. A total of 1,358 ASVs were identified from the ITS data from all soil samples. The 16S rRNA amplicon data indicates the Proteobacteria and Acidobacteriota (formerly Acidobacteria, all nomenclature will follow GTDB from this point forward) were the most abundant phyla in the soil, comprising an average of 40.5% and 21.3% of total reads (Figure 3.3A). The fungal ITS data was dominated by the Ascomycota, at an average abundance of 96.4% (Figure 3.3B). Little variation across column (fertilizer), depth, or time was observed (Figure 3.4, Figure 3.5, Figure 3.6) except for the Acidobacteriota, whose abundance drops from 24.3% to 21.1%, and then to 17.6% sequentially across phase with a significant difference (by Tukey HSD test; $p = 0.0116$) between pre- and post-FTC. Lineages previously identified as susceptible to freeze-thaw stress, including Proteobacteria and Actinobacteriota (formerly Actinobacteria), changed negligibly across phase from pre, during, and post-FTC (Žifčáková et al., 2016; Han et al., 2018a; Ren et al., 2018). In non-significant changes, Proteobacteria decreased from 42.6% relative abundance to 39.9–40.0%, and Actinobacteriota increased from 9.7% to 11.8–14.7% (Figure 3.3A). Ascomycota is the sole fungal phylum that decreased significantly (by Tukey HSD test; $p = 0.0362$ and $p = 0.0069$) from 96.1 to 97.2%–93.8% (Figure 3.3B). Actinobacteriota enriched over the

experiment as a general trend, but at the shallowest depth, which experienced FTC, this enrichment diminishes in magnitude, with a change from 8.6–11.2%–11.2% and does not represent a significant difference by Tukey HSD (Figure 3.5A). Similarly, Ascomycota at the shallowest depth changes only from 96.6–97.8%–96.0% and does not represent a significant change by Tukey HSD. Changes in the Proteobacteria and Ascomycota were consistent across the depth profile of the columns. Lack of community response at the phylum level led to analysis of lower taxonomic ranks, which revealed similar muted changes with no clear connection to fertilizer, depth, or temperature conditions.

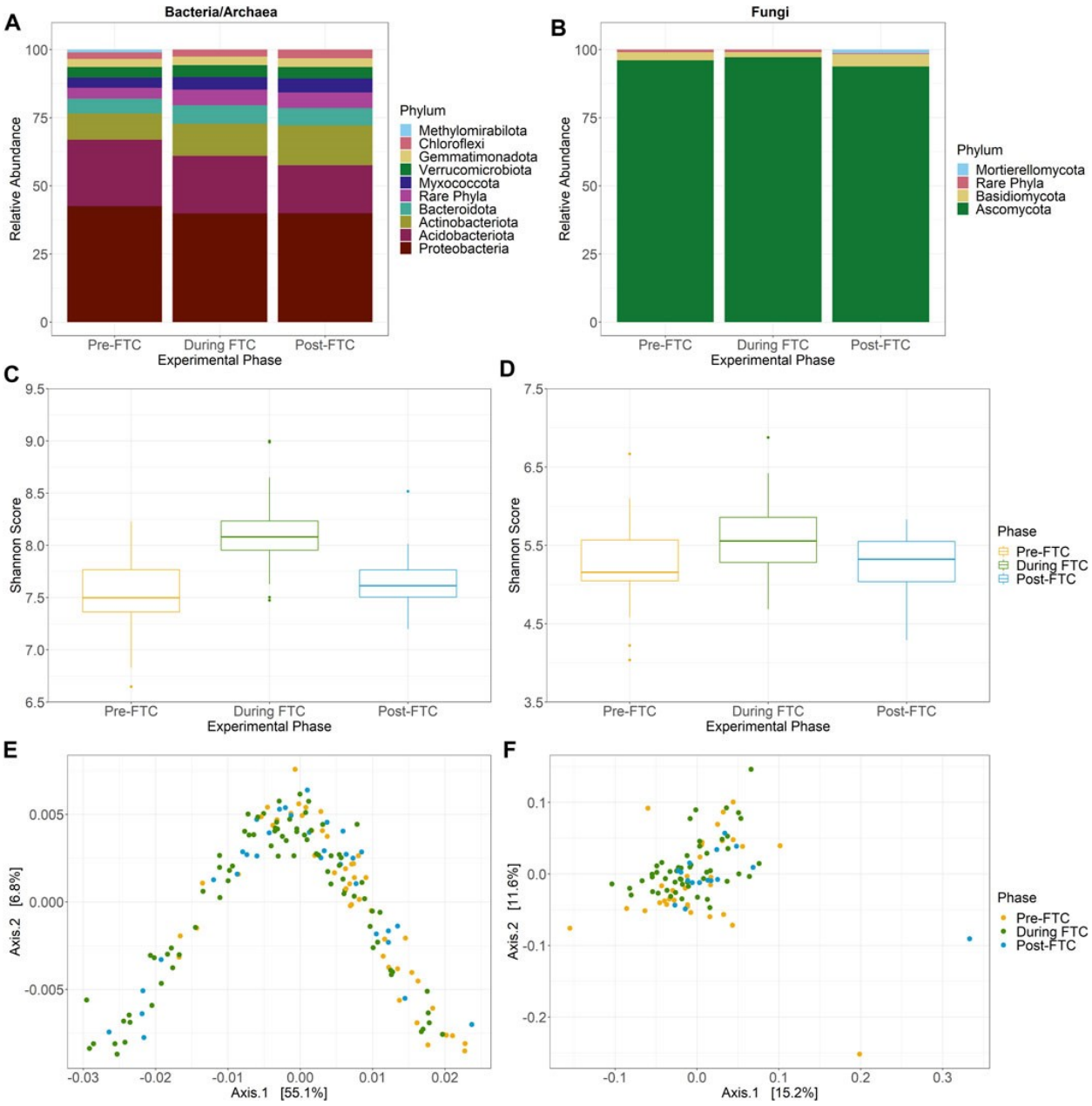

Figure 3.3: Community composition and diversity across phase. Bacterial and archaeal (A), and fungal (B) community composition at the phylum level across FTC phases. ASVs identified from QIIME2 were then classified using the Silva 138 99% OTUs (A) or UNITE 8.2 99% dynamic OTUs (B) reference sequences. "Rare phyla" encompass all phyla below 1% relative abundance. The bacterial/archaeal community are dominated by Proteobacteria and Acidobacteriota with diminishing abundance of the Acidobacteriota and increasing abundance of Actinobacteriota over time. The fungal community is predominately Ascomycota with little observed variation

over time. (C,D) Bacterial and archaeal (C), and fungal (D) alpha diversity Shannon score across FTC phases in boxplot distributions collapsing column, depth, and time into phases. Significant differences, detected by the Tukey HSD test, distinguish the During FTC phase from the others among the bacterial and archaeal community but no such difference exist for the fungal community. Bacterial and archaeal (E), and fungal (F) beta diversity by PCoA generated with weighted Unifrac distances across FTC phases. Principal axis for the bacterial/archaeal community account for a high degree of variation and possess a distinct horseshoe shape with slight separation by phase. Little variation is explained for any principal axis in the fungal community and sites do not appear to cluster by phase.

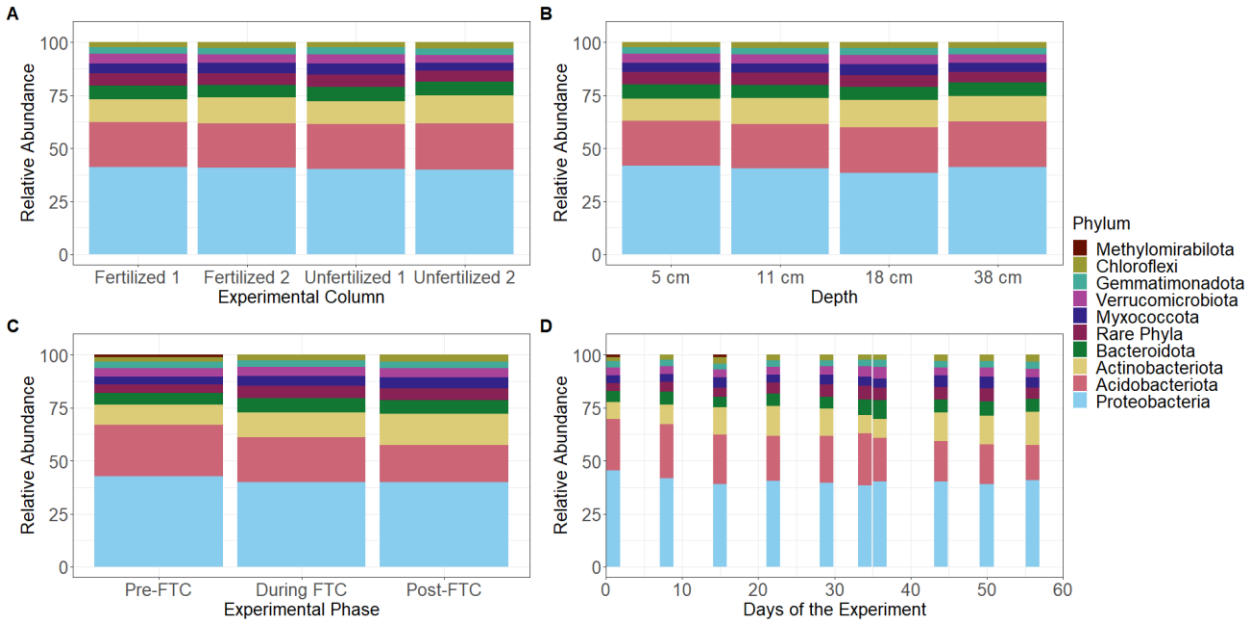

Figure 3.4: Bacterial and archaeal phylum-level community composition across column, depth, and time. Bacterial and archaeal ASVs identified from QIIME2 were then classified using the Silva 138 99% OTU reference sequences and are shown at the phylum level across categorical variables. The "Rare phyla" category encompasses all phyla below 1% relative abundance. Dominant phyla include Proteobacteria and Acidobacteriota with little observed variation in phylum abundances across column (fertilizer) and depth. Across time there appears to be an increase of Actinobacteriota and a decrease in Acidobacteriota.

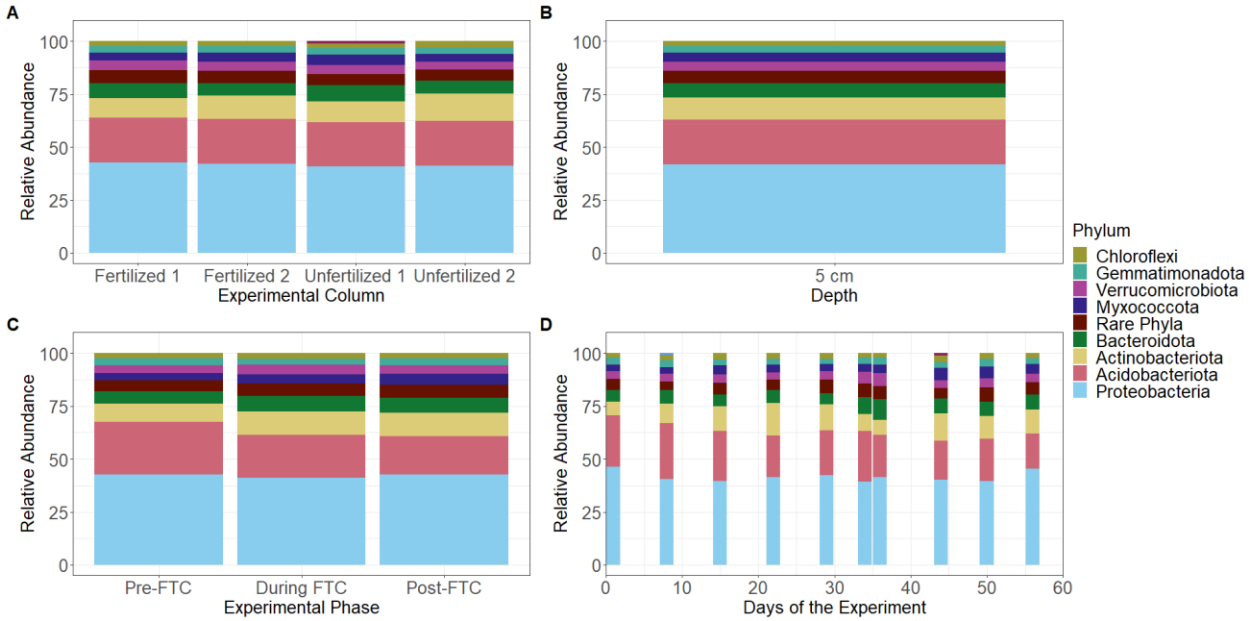

Figure 3.5: Bacterial and archaeal phylum-level community composition from the 5 cm depth samples across column, depth, and time. Samples were first subset to those from the first 5 cm depth that experienced freeze-thaw stress. Then bacterial and arachaeal ASVs identified from QIIME2 were classified using the Silva 138 99% OTU reference sequences and shown at the phylum level across categorical variables. The "rare phyla" category encompasses all phyla below 1% relative abundance. Dominant phyla include Proteobacteria and Acidobacteriota with little observed variation in phylum abundances across column (fertilizer), and time.

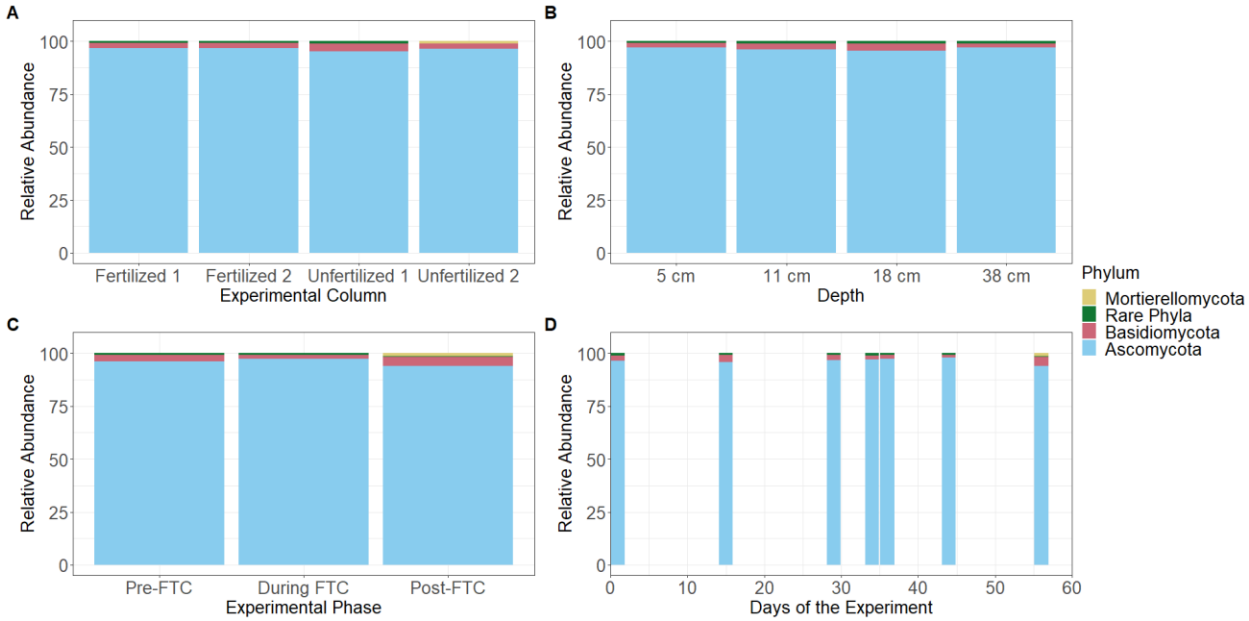

Figure 3.6: Fungal phylum-level community composition across column, depth, and time. Fungal ASVs identified from QIIME2 were then classified using UNITE 8.2 99% dynamic OTUs reference sequences and are shown at the phylum level across categorical variables. "Rare phyla" encompass all phyla below 1% relative abundance. The communities are largely dominated by Ascomycota with little observed variation in abundance across column (fertilizer), depth, and time.

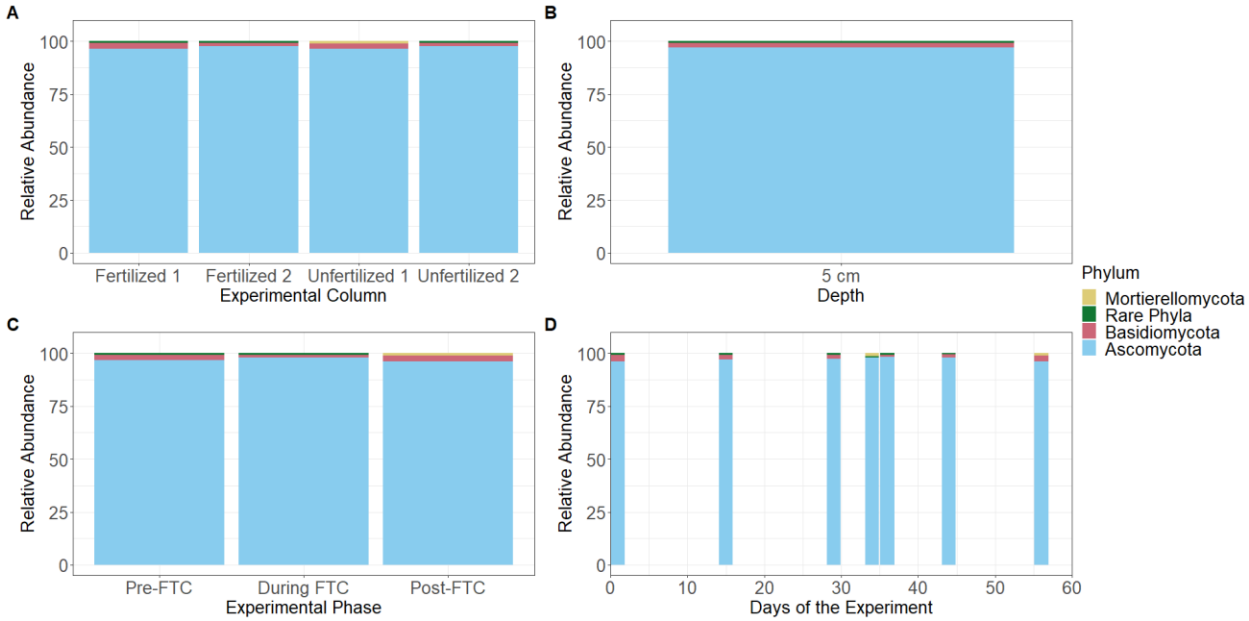

Figure 3.7: Subsurface fungal phyla community composition across column, depth, and time. Samples were first subset to those from the first 5 cm depth that experienced freeze-thaw stress. Fungal ASVs identified from QIIME2 were then classified using UNITE 8.2 99% dynamic OTUs reference sequences and shown at the phyla level across categorical variables. Rare phyla encompass all phyla below 1% relative abundance. Phyla are largely dominated by Ascomycota with little observed variation in abundance across column (fertilizer), and time.

Genus level changes appear similarly muted across experimental phase. Bacterial and archaeal genera differed in relative abundance by a median of 17.3% within their proportion of the community composition (e.g., from 1.0% to 1.17%) between adjacent phases, with the exception of *Pseudomonas* which dropped from 2.8% to 0.5% of the community after the onset of FTC, a 82% drop in relative abundance (Figure 3.8). The fungal genera were more variable than bacteria and archaea with a median 25% change in relative abundance within their proportion of the community composition (e.g., from 2% to 2.5%) across adjacent phases (

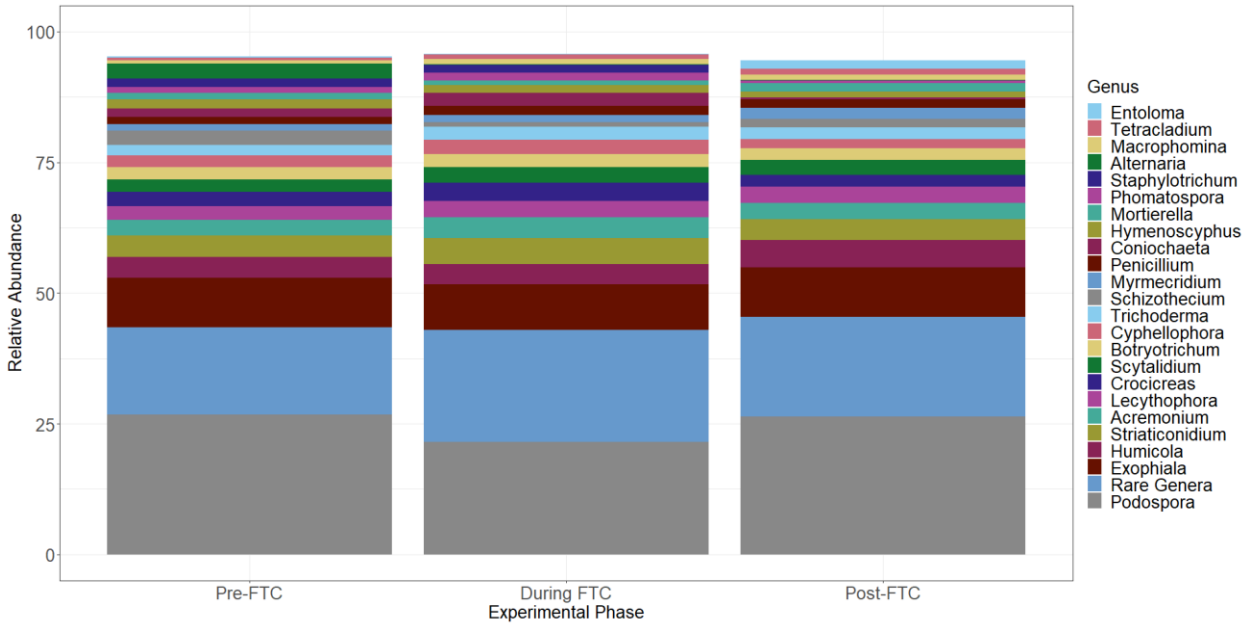

Figure 3.9). The higher variance in the fungal data may have been impacted by the lower sampling frequency. Dominant fungal genera are those of the Ascomycota phyla including the *Podospora* and *Entoloma* genera.

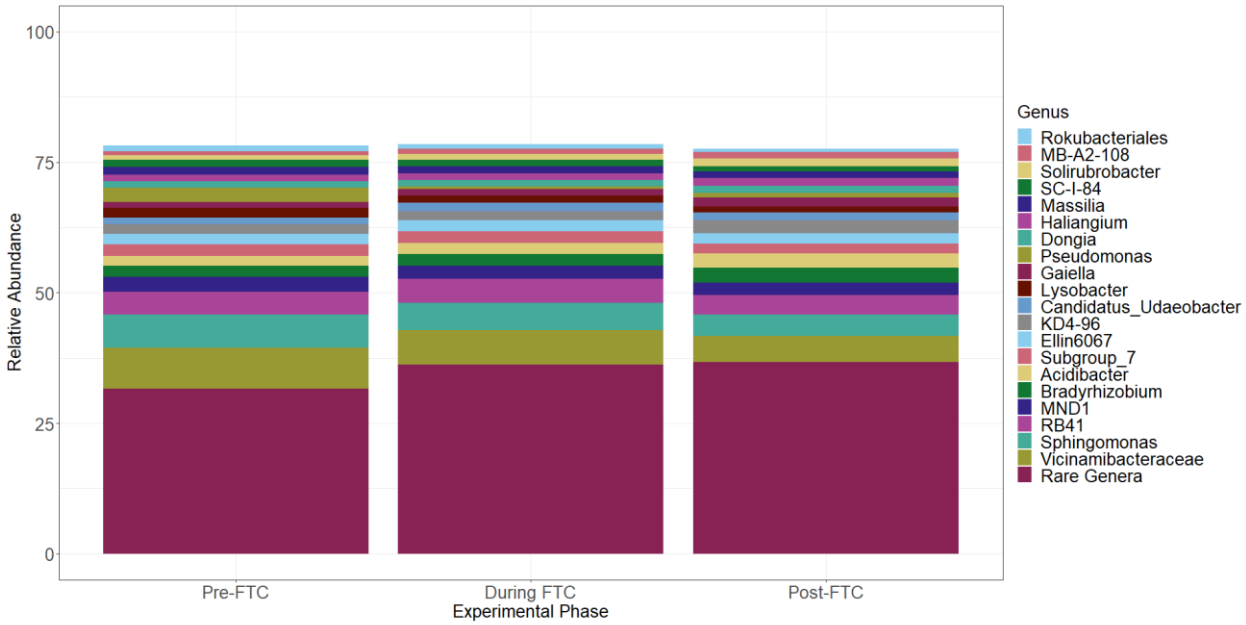

Figure 3.8: Bacterial and arachaeal ASVs identified from QIIME2 were classified using the Silva 138 99% OTU reference sequences and are shown at the genus level across phase. The

"Rare Genera" category encompasses all genera below 1% relative abundance in all experimental phases. ASVs not resolved to the genus level were excluded. Genera abundances across phase had a median deviation of 17.3% of their proportion of the community (e.g., from 1.0% to 1.17%) between adjacent experimental phases.

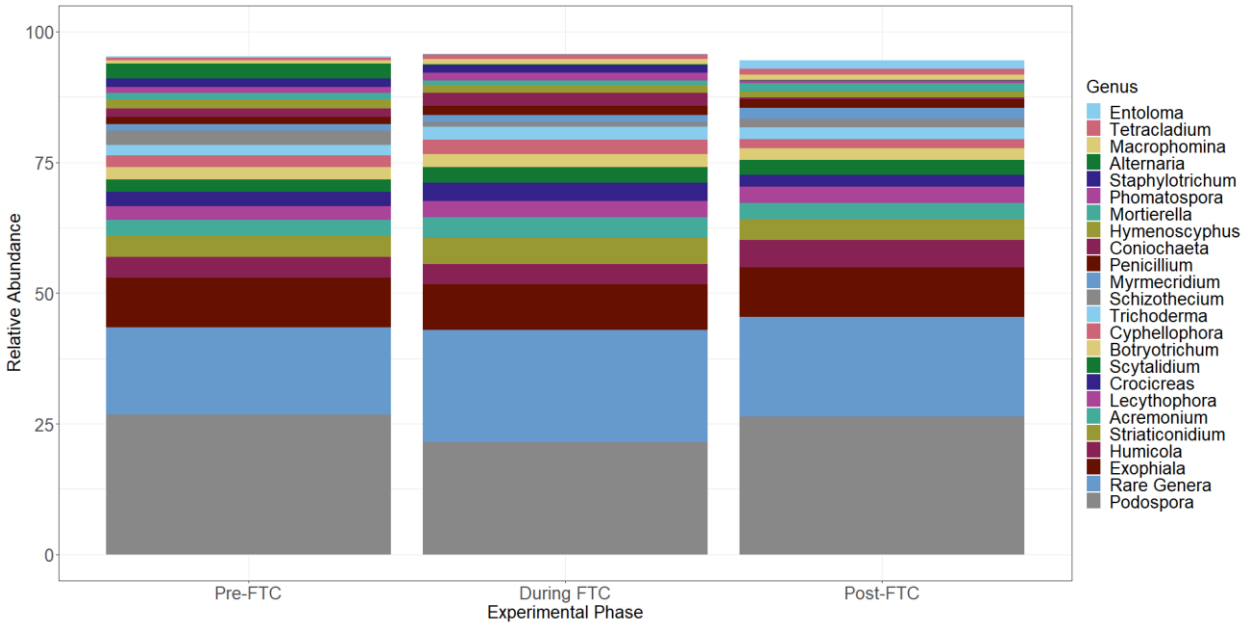

Figure 3.9: Fungal ASVs identified from QIIME2 were classified using the Silva 138 99% OTU reference sequences and shown at the genus level across phase. The "Rare Genera" category encompasses all genera below 1% relative abundance in all experimental phases. ASVs not resolved to the genus level were excluded. Genera abundances across phase showed a median deviation of 25.0% of their proportion of the community composition (e.g., from 2% to 2.5%) between adjacent experimental phases. Genera are largely dominated by *Podospora* and *Exophiala*, members of the Ascomycota phyla.

3.3 Alpha Diversity

Changes in alpha diversity were assessed for disruption due to fertilizer amendment and FTC. No discernible or intuitive trend for bacterial/archaeal alpha diversity was observed that was consistent across fertilizer or depth conditions (Figure 3.10), however an overall increase in alpha diversity is observed for aggregated samples within the FTC phase (Figure 3.3C). The

5 cm depth, which was experiencing FTC, showed similar magnitudes and patterns for alpha diversity (Figure 3.11). An ANOVA performed across categorical variables only identified phase as significant, with neither column (fertilizer) nor depth resulting in changes to richness or evenness. Within the phase variable, a Tukey HSD test for observed ASVs and Shannon Index identified only samples during freeze-thaw cycling as significantly different from pre- and post-FTC, as a noticeable increase in diversity is observed over phase but then returns to pre-FTC levels after temperature fluctuations cease. In contrast, Faith's PD showed significant differences for each phase (Figure 3.10). This difference between the pre- and during FTC was consistent for all sampling depths, but at the 5 cm depth was not significant between any other groupings, as the drop in diversity post-FTC was lower in magnitude (Figure 3.11). This was unexpected, as freeze-thaw stress was expected to act as a greater selection process for microbes less capable of cold shock adaption. Instead, we observed an increase in diversity during FTC and then a return to the pre-FTC magnitude. This may represent an enrichment of rare ASVs in response to newly available labile carbon from cell lysis.

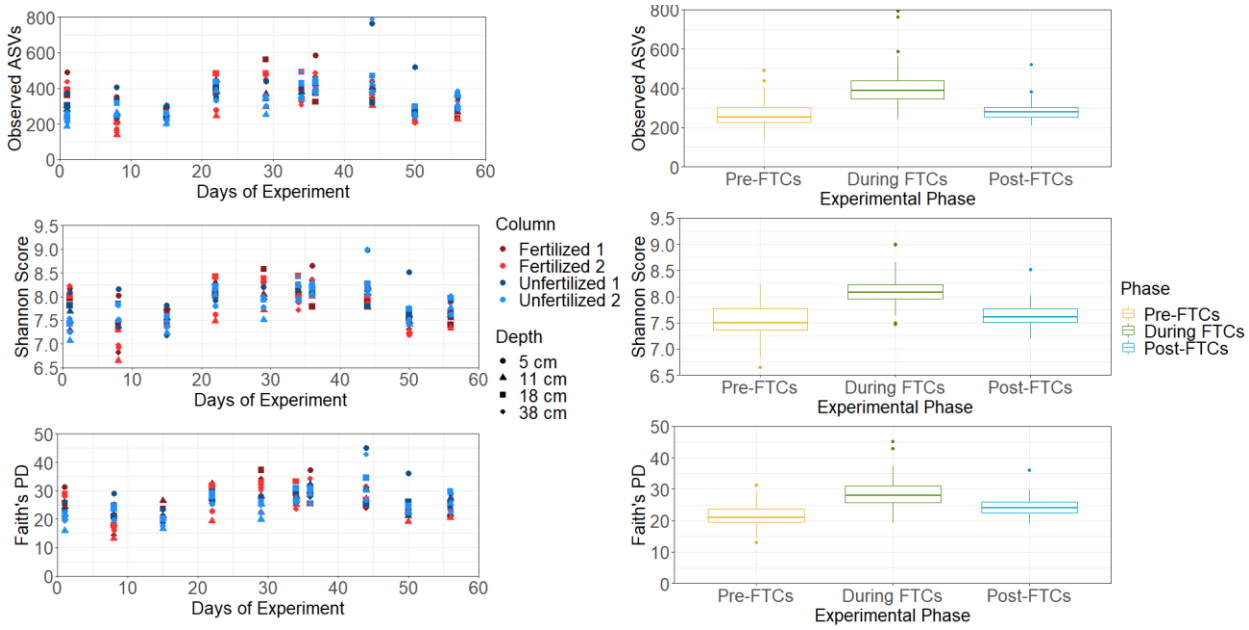

Figure 3.10: Bacterial and archaeal alpha diversity across time and phase. Left: Metrics of alpha diversity including observed ASVs, Shannon score, and Faith's Phylogenetic Distance are shown for each individual soil extract across all columns, depths, and time. Right: Boxplot distributions collapsing column, depth, and time into phases.

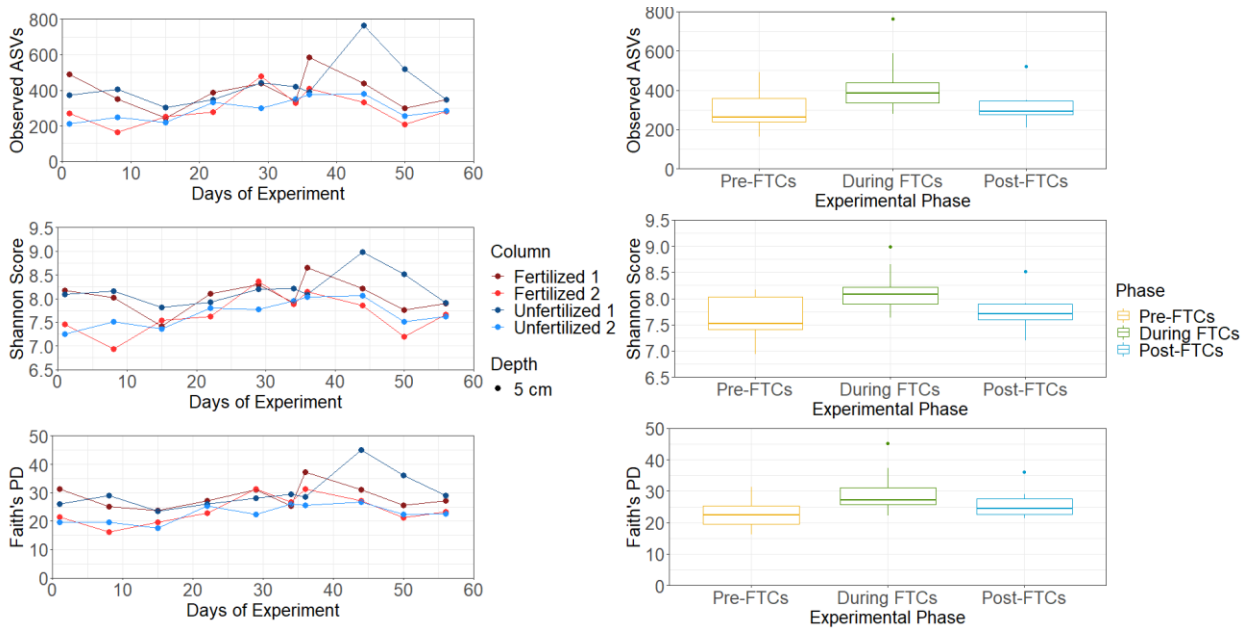

Figure 3.11: Bacterial and archaeal alpha diversity across time and phase for the 5 cm depth samples. Left: Metrics of alpha diversity including observed ASVs, Shannon score, and Faith's Phylogenetic Distances are shown for the 5 cm sample for each individual soil extract from all depths, and time. Right: Boxplot distributions collapsing column and time into phases.

Meanwhile the fungal community experienced a much more muted change. Similarly, there were no significant changes in all metrics of alpha diversity associated to fertilizer treatment, depth, or phase (Figure 3.3D; Figure 3.12) with the same true at the 5 cm depth (Figure 3.13). However, it is interesting to note that while there is overall lower diversity among the fungal community in observed ASVs and Shannon score there are similar Faith's PD levels between the fungal and bacterial/archaeal community, indicating that while the fungal community is less diverse at an ASV level, the ASVs are less closely related.

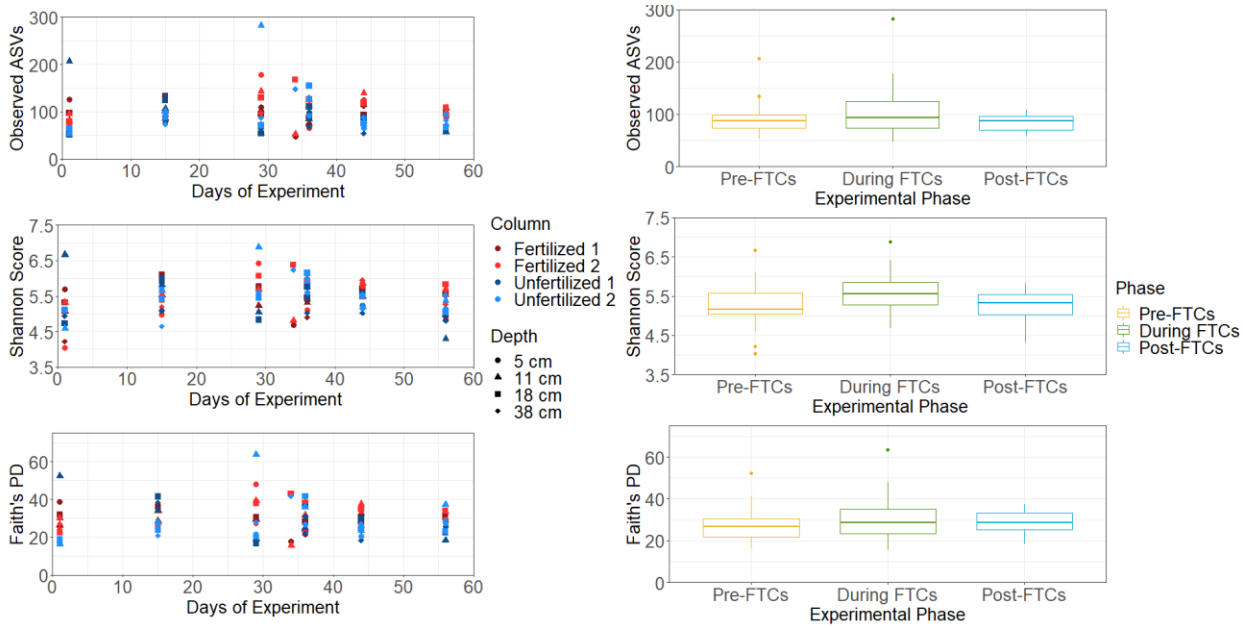

Figure 3.12: Fungal alpha diversity across time and phase. Left: Metrics of alpha diversity including observed ASVs, Shannon score, and Faith's Phylogenetic Distance are shown for individual soil extracts from all columns, depths, and time. Right: Boxplot distributions collapsing column, depth, and time into phases.

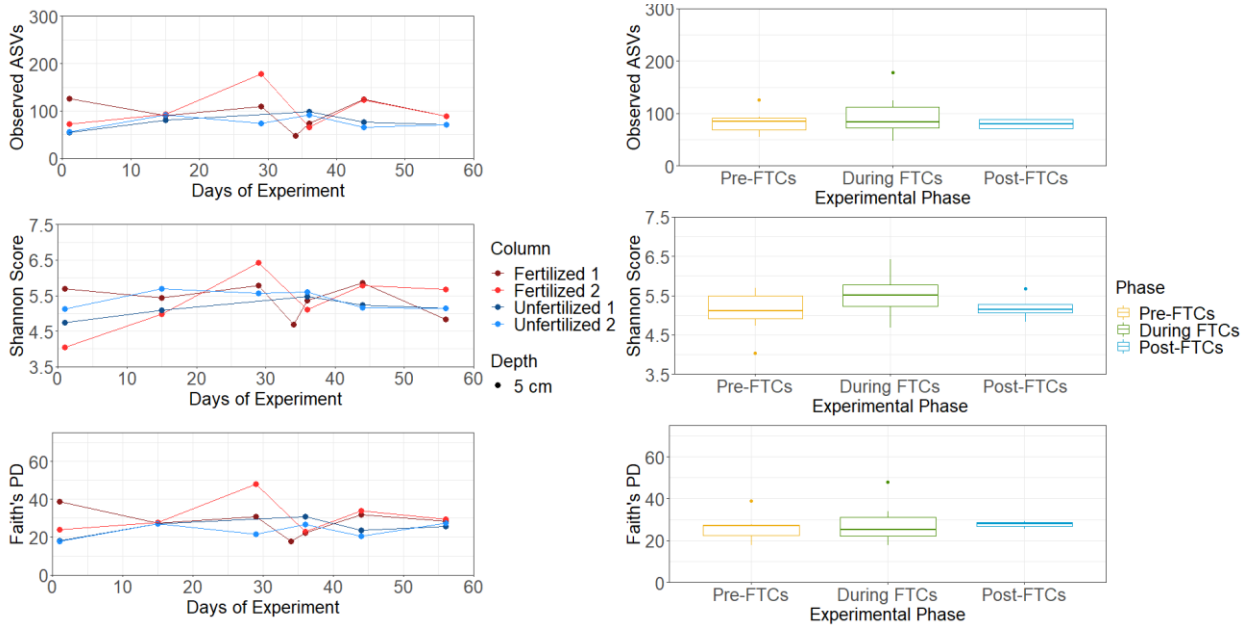

Figure 3.13: Fungal alpha diversity across time and phase in the 5 cm depth. Left: Metrics of alpha diversity including observed ASVs, Shannon score, and Faith's Phylogenetic Distance are

shown for the 5 cm subsurface for each individual soil extracts from all depths, and time. Right: Boxplot distributions collapsing column and time into phases.

3.4 Beta Diversity and Canonical Ordination

Beta diversity values did not demonstrate a clear relationship with column (fertilizer), depth, or across phase for either the bacterial/archaeal or the fungal communities (Figure 3.14, Figure 3.15). One exception was for the bacterial and archaeal community using weighted Unifrac distances (Figure 3.3E). When visualized as a two-dimensional PCoA the samples form a distinct horseshoe shape, with 55.1% of the total variation captured by the primary axis. Direct comparison using unweighted and weighted Unifrac distances showed the weighted contribution of relative abundance is necessary to reveal this pattern (Figure 3.16). Taken together, the combination of relative abundance and phylogenetic diversity must be required to identify this pattern, as it is not evident with Bray-Curtis distances, which incorporate relative abundance, or with unweighted Unifrac, which also use phylogenetic diversity. Within the weighted Unifrac distribution, samples are loosely ordered by phase along the principal axis (Figure 3.3E). Examination of solely the −5 cm depth samples revealed no deeper insight except that the horseshoe shape among the bacterial/archaeal samples was retained (Figure 3.17, Figure 3.18).

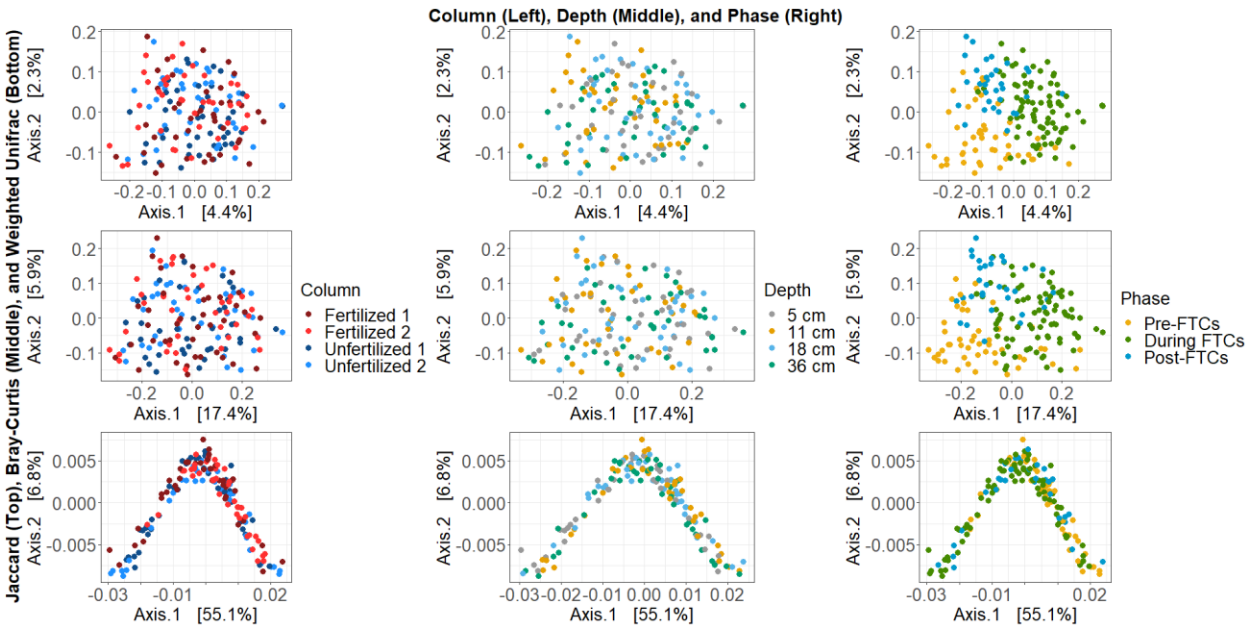

Figure 3.14: Bacterial and archaeal beta diversity ordination of sites via PCoA. PCoAs were generated from Jaccard (top), Bray-Curtis (middle), and Weighted Unifrac (bottom) distance metrics, visualized with points for each specific site highlighted accordingly across categorical variables: Left: column, center: depth, right: phase. For Jaccard and Bray-Curtis, only minor variation is explained by the principal axes and sites do not cluster to any significant degree with either column (fertilizer), depth, or phase. Weighted Unifrac is the exception with a higher degree of variation on its principal axis and distinct horseshoe shape, but only a minor trend in distribution based on phase observed with pre-FTCs only appearing on one side of the horseshoe with equal distribution of the other phases.

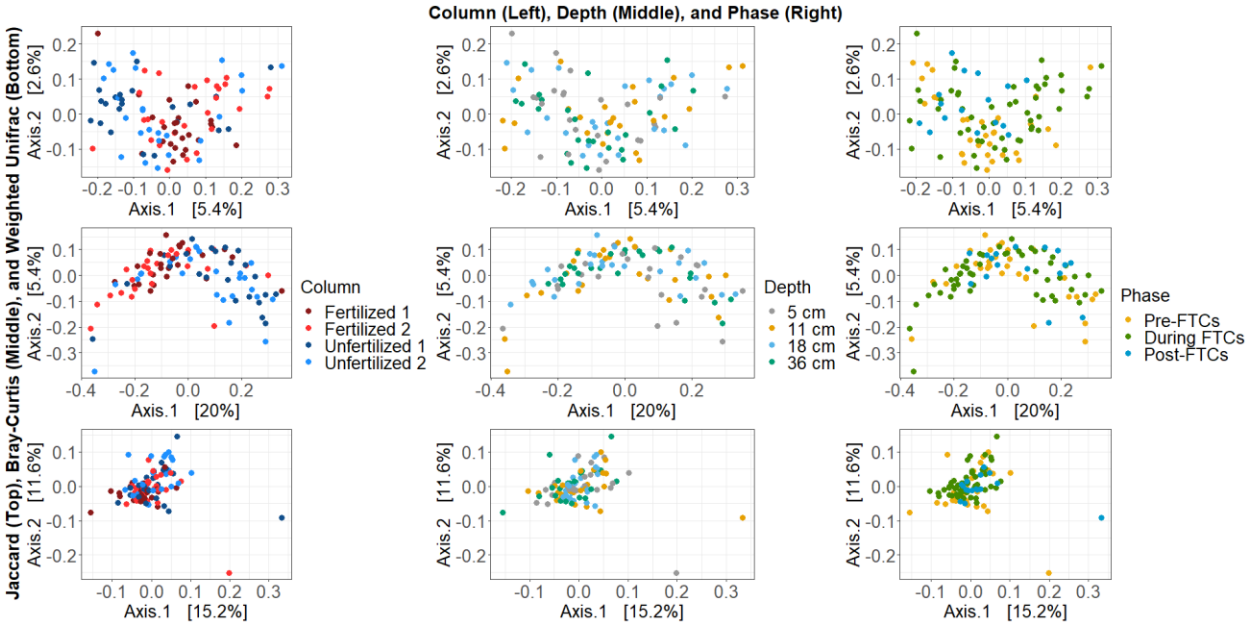

Figure 3.15: Fungal beta diversity ordination of sites via PCoA. PCoAs were generated from Jaccard (top), Bray-Curtis (middle), and Weighted Unifrac (bottom) distance metrics, visualized with points for each specific site highlighted accordingly across categorical variables: Left: column, center: depth, right: phase. Little variation is explained for any principal axis and sites do not cluster to any significant degree with either column (fertilizer), depth, or phase.

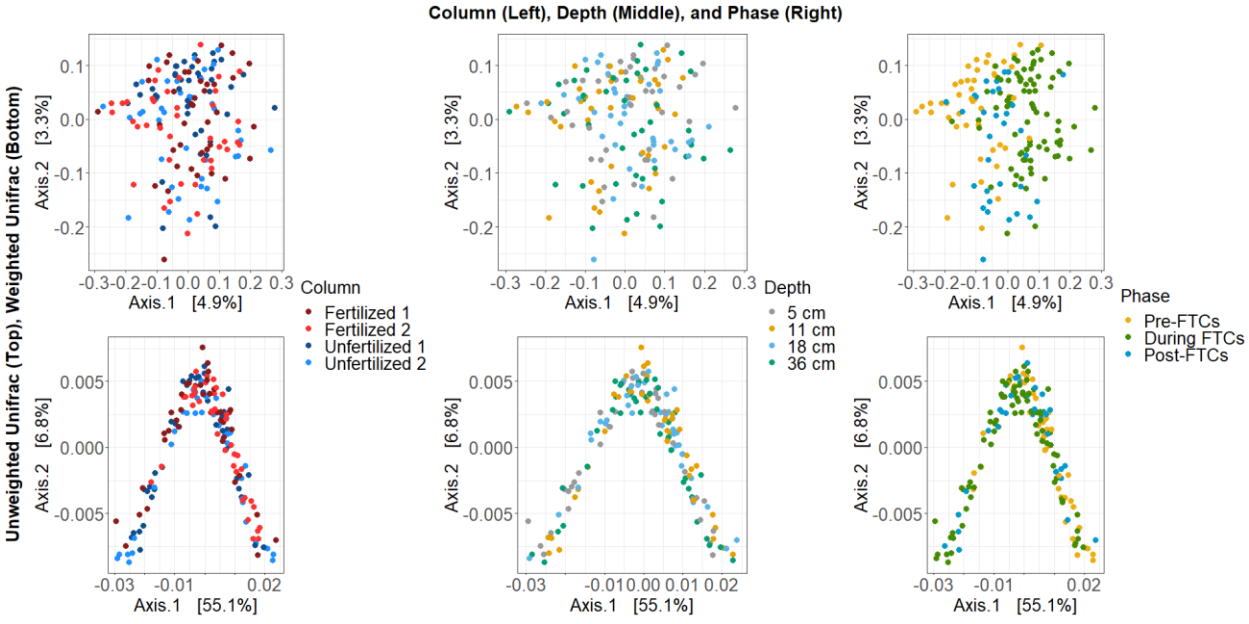

Figure 3.16: Bacterial and archaeal beta diversity ordination of sites via PCoA of weighted and

unweighted Unifrac**.** PCoAs were generated from unweighted Unifrac (top) and weighted Unifrac (bottom) distance metrics, visualized with points for each specific site highlighted accordingly across categorical variables: Left: column, center: depth, right: time. Weighted Unifrac ordinations reveal a horseshoe shape with a higher degree of variation encapsulated in its principal axis at 55% with a minor trend in the time variable.

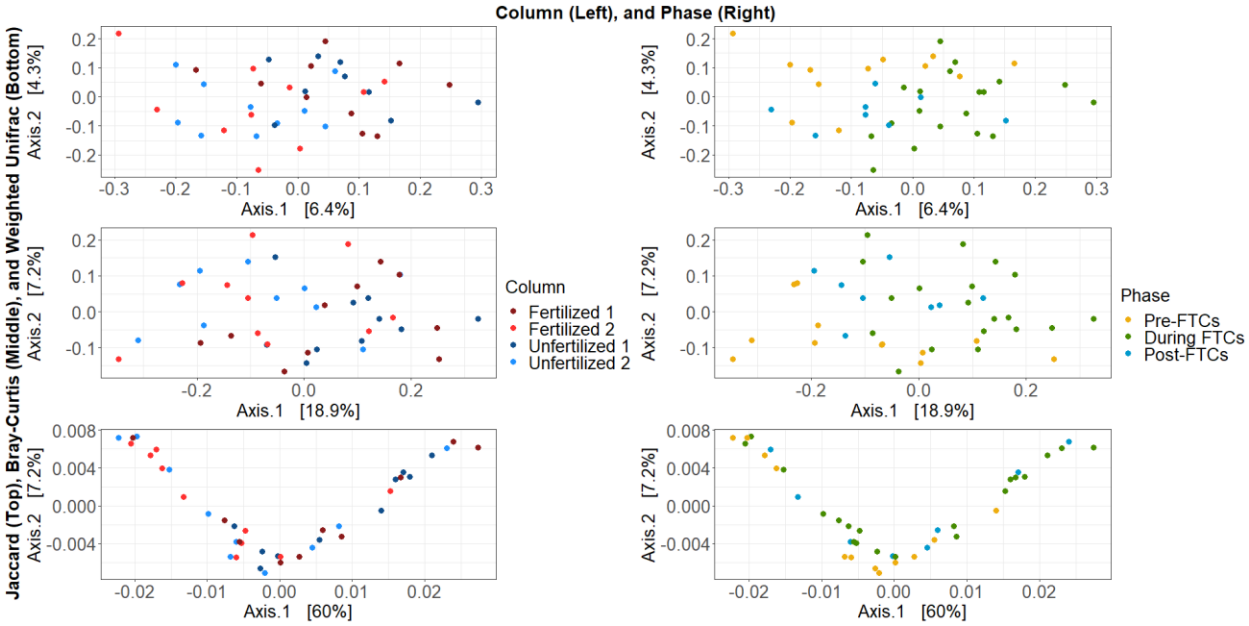

Figure 3.17: Bacterial and archaeal beta diversity ordination of sites via PCoA for the 5 cm depth. Data was first subset to the first 5 cm of soil depth and then PCoAs were generated from Jaccard (top), Bray-Curtis (middle), and Weighted Unifrac (bottom) distance metrics, visualized with points for each specific site highlighted accordingly across categorical variables: Left: column, center: depth, right: phase. For Jaccard and Bray-Curtis, only minor variation is explained for any principal axis and sites do not cluster to any significant degree with either column (fertilizer), or phase. Weighted Unifrac is the exception with a higher degree of variation on its principal axis and distinct inverted horseshoe shape.

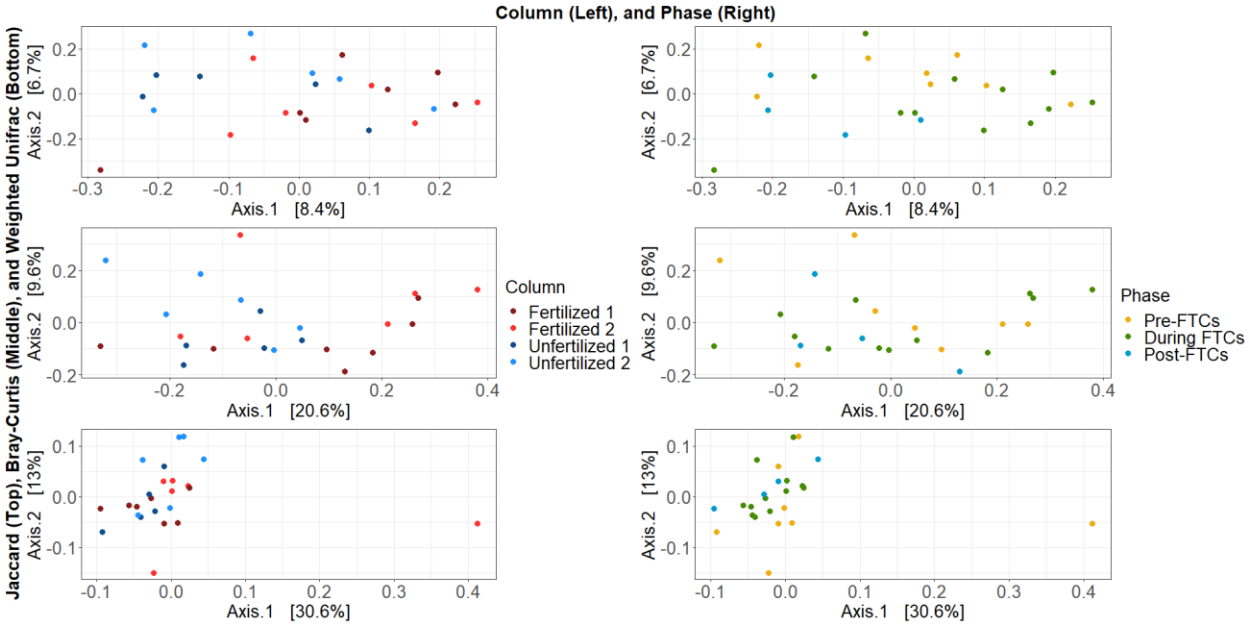

Figure 3.18: Fungal beta diversity ordination of sites via PCoA for the 5 cm depth. Data was first subset for the first 5 cm of soil depth and then PCoAs were generated from Jaccard (top), Bray-Curtis (middle), and Weighted Unifrac (bottom) distance metrics, visualized with points for each specific site highlighted accordingly across categorical variables: Left: column, center: depth, right: phase. Little variation is explained for any principal axis and sites do not cluster to any significant degree with either column (fertilizer), or phase.

Given the temporal variable was associated with beta diversity differences, we focused on identifying the role of phase in the bacterial and archaeal samples through a canonical ordination to determine the contribution of environmental and categorical variables in distinguishing the microbial community compositions across sample sites. Continuous variables were captured in nMDS plots (Figure 3.19A) and categorical variables in CCA plots (Figure 3.19B).

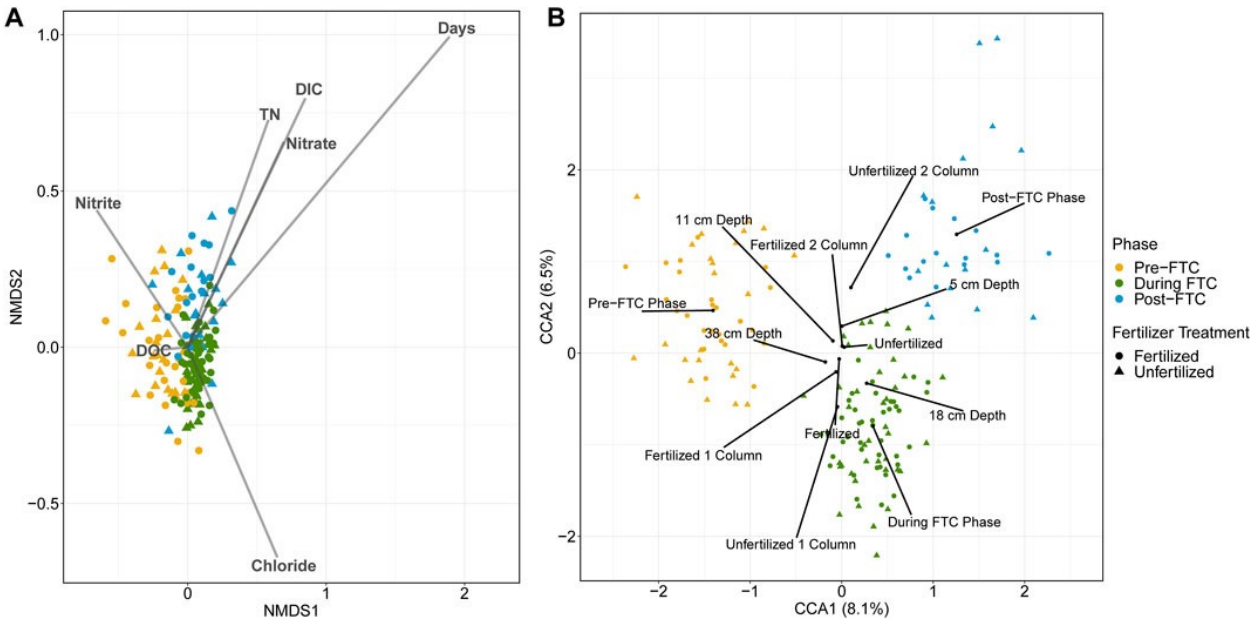

Figure 3.19: Bacterial and archaeal canonical ordination. Ordinations are generated from Bray-Curtis distances of all 7390 ASV relative abundances across all 160 soil samples. Samples are indicated by colour for the phase of freeze-thaw cycling (yellow for pre-FTC; green for during FTC; blue for post-FTC), and shape for fertilizer treatment (circle for fertilized; triangle for unfertilized). An nMDS plot (A) with vectors representing time as well as geochemical variables obtained from the soil leachate overlayed. Time is the largest continuous variable contributor to sample dissimilarity with the largest vector and the samples clearly segregated by phase of freeze-thaw cycling. A CCA plot (B) with centroids representing the factor levels of categorical variables including phase, depth, column, and fertilizer are shown. The strongest categorical variable for influencing sample dissimilatory is phase, indicated by segregated samples by phase. Despite this, the two principal coordinate axes explain only 6.5 and 8.1% of the variation in the samples.

For the bacterial and archaeal samples, the strongest indicator variable in the nMDS and CCA plots are both elements of time: 'Days' on the nMDS ($p = 0.001$, $r^2 = 0.4560$; Figure 3.19A), and the phases' centroids on the CCA ($R = 0.4858$, $p = 0.0001$; Figure 3.19B). This adds to the observed trend in alpha and beta diversity metrics of specific, limited differences in the microbial

communities aligning with the phase of the temperature regime. There was little explanatory power assigned to any of the other variables. For example, significant variables on the nMDS showed weak environmental fitting: dissolved inorganic carbon (DC) ($p = 0.001$; $r^2 = 0.1356$), total nitrogen (TN) ($p = 0.002$; $r^2 = 0.0860$), Cl^- ($p = 0.002$; $r^2 = 0.0871$), NO_2^-($p = 0.010$; $r^2 = 0.0625$), and NO_3^- ($p = 0.001$; $r^2 = 0.0915$). Significance and magnitude of dissimilarities between microbial communities across sample types was assessed using the ANOSIM test. This showed that, while the factors depth ($R = 0.0209$; $p = 0.01$), column ($R = 0.0621$; $p = 0.0001$), and fertilizer ($R = 0.0285$; $p = 0.0023$) were significant, most possess a low R-statistic revealing little contribution to the magnitude of community dissimilarity. When run on a model accounting for fertilizer, column, depth, and phase, the CCA captured only a small percentage of variation associated with its principal axes (8.1 and 6.5%; Figure 3.19B), and the only meaningful separation can be explained by phase of freeze-thaw cycling.

For the fungal samples, the ordination from the nMDS identified only NO_3^- ($p = 0.014$; $r^2 = 0.0956$) and TN ($p = 0.014$; $r^2 = 0.0956$) as significant variables, although these contribute negligibly to the explanatory power of sample separation (Figure 3.20). Unlike the bacterial and archaeal samples, separation of samples along fertilizer or phase variables is not observed (Figure 3.3F). Significance and magnitude of dissimilarities between microbial communities across sample types assessed using the ANOSIM test showed that only factors of phase ($R = 0.1607$; $p = 0.0003$), column ($R = 0.0221$; $p = 0.0386$), and fertilizer ($R = 0.0309$; $p = 0.0084$) were significant, but all possess a low R-statistic revealing little contribution to the magnitude of community dissimilarity. When run on a model accounting for fertilizer, column, depth, and phase, the CCA captured only a small percentage of variation associated with its principal axes (11.3 and 13.0%; Figure 3.21). For this reason, analyses past this point emphasized tracking

changes to the designated core microbiomes and potential predicted nitrogen cycling communities identified by PICRUSt2.

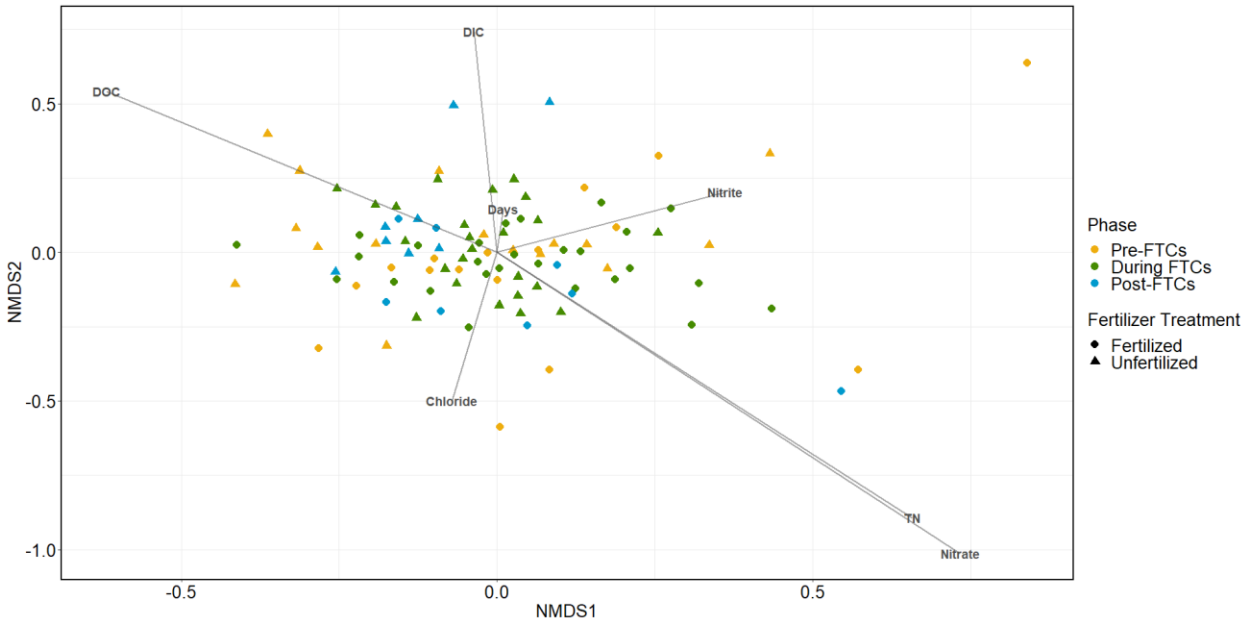

Figure 3.20: Fungal ordination of samples via nMDS. The nMDS plot was generated from Bray-Curtis distances of all 1,358 ASV relative abundances across 99 soil samples. Samples are indicated by colour for the phase of freeze-thaw cycling (yellow for pre-FTCs; green for during FTCs; blue for post-FTCs), and shape for fertilizer treatment (circle for fertilized; triangle for unfertilized). Vectors representing time as well as geochemical variables obtained from the soil leachate are overlayed. Nitrate represents the strongest factor for sample dissimilarity however no evident sample grouping across phase or fertilizer condition is observed.

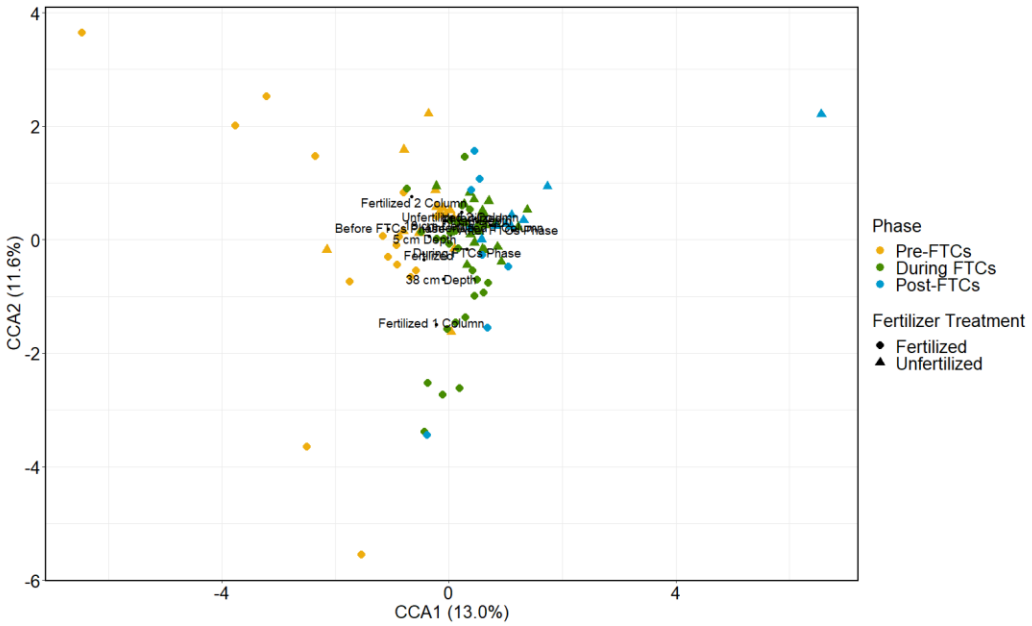

Figure 3.21: Fungal ordination of samples via CCA. The CCA plot was generated from Bray-Curtis distances of all 1,358 ASV relative abundances across 99 soil samples. Samples are indicated by colour for the phase of freeze-thaw cycling (yellow for pre-FTCs; green for during FTCs; blue for post-FTCs), and shape for fertilizer treatment (circle for fertilized; triangle for unfertilized). Centroids representing the factor levels of categorical variables including phase, depth, column, and fertilizer are shown. Some sample variation is evident from phase although with a less distinct grouping as for the bacterial and archaeal samples.

3.5 Abundance-Occupancy "Core" Modeling

Bacterial, archaeal, and fungal ASVs were assigned to a "core" microbiome predicated on their unique temporal site specific abundance and occupancy across all extracted soil samples as described by Shade and Stopnisek (2019). ASVs were first ranked based on the abundance-occupancy distribution of all samples and then core members were sequentially included iteratively if their explanatory power towards Bray-Curtis dissimilatory of the community increases beyond the designated threshold (see Materials and Methods for more detail). The stability of the core community was then assessed via its changing relative abundance with time.

The bacterial core community was composed of 94 ASVs from an original 7,390 ASVs, accounting for 25% of the total beta diversity, which constitutes a meager majority of the community with 45–50% summed relative abundance (Figure 3.22). The community composition of the core generally resembled the total community and is predominantly made up of Proteobacteria and Acidobacteriota (Figure 3.23). A decline in the core community's abundance occurs during FTC with a recovery afterwards (Figure 3.22A). Tukey HSD tests for multiple pairwise comparisons identified that, within both fertilized and unfertilized treatments, the phase change between pre- and during FTC, and between during and post-FTC showed significant changes to the core community's shared abundance. The two fertilizer treatments significantly differed only in the post-FTC phase, in which the fertilizer treatments showed an elevated core abundance. These shifts in core community composition appear indirectly related to freeze-thaw stress, as these significant differences were not observed for the 5 cm depth (Figure 3.24). For the 5 cm depth, only the shift between the during and post-FTC phases was significant.

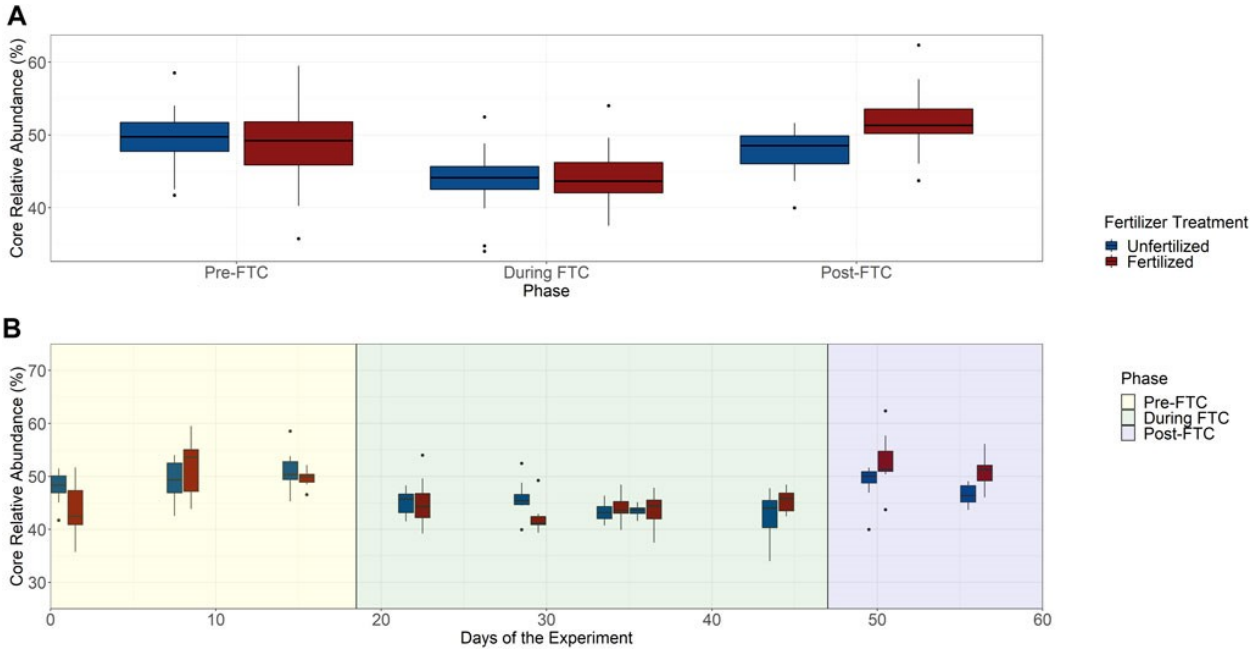

Figure 3.22: Bacterial and archaeal core community. The total community abundance of the 94 ASVs identified as the core community were plotted over phase with fertilized and unfertilized treatments plotted separately (A). Tukey HSD tests for multiple pairwise comparisons identified significant differences associated with pre- and during FTC, and during and post-FTC within both fertilizer treatments. Relative abundance recovers post-FTC, and the pre- and post- FTC phases were not significantly different. Fertilizer treatments do not seem to differ within a phase except post-FTC where the fertilizer sample is significantly elevated. The difference in mean relative abundance is ~5% from pre- to during FTC and recovers post-FTC by ~4% by the unfertilized and ~5% for the fertilized. The total community relative abundance of the 94 ASVs identified for core community inclusion is plotted over time with treatments of unfertilized and fertilized columns plotted separately (B). Adjacent time-points and fertilizer treatments do not show significant variation. The core community appears unaltered in relative community abundance under freeze-thaw or nutrient induced stress.

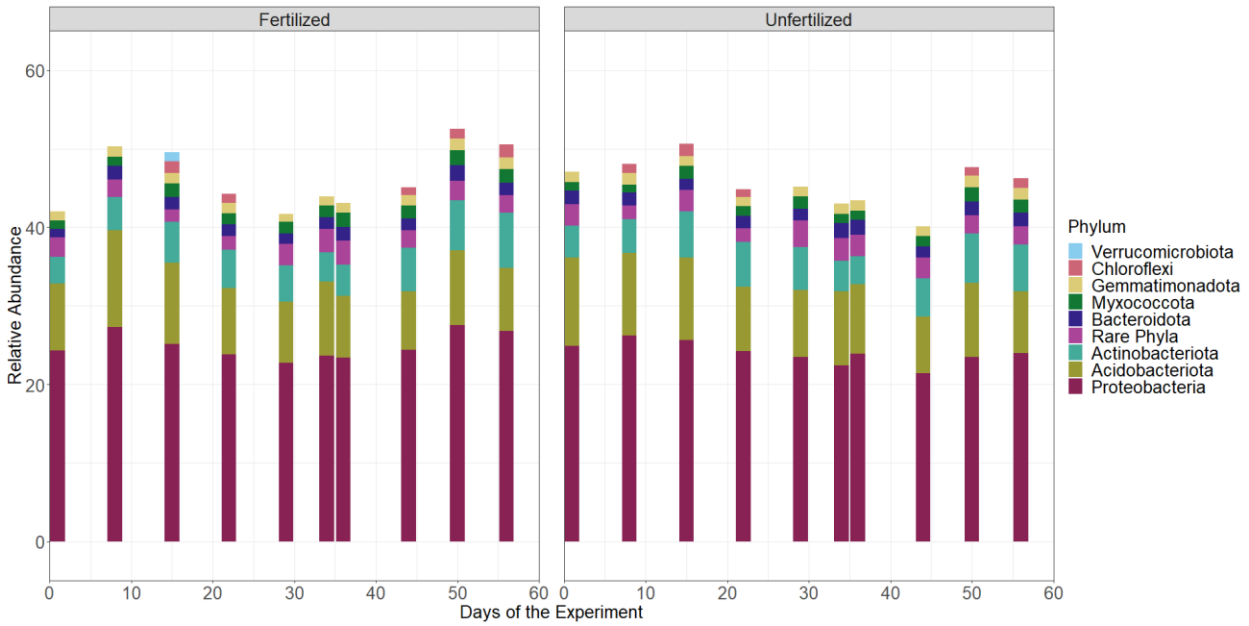

Figure 3.23: Bacterial and archaeal core community composition by major phyla over time, with fertilizer treatments presented separately. The total community relative abundance of the 94 ASVs identified for core community inclusion were plotted over time and faceted across fertilizer treatments. The "Rare phyla" category comprises the sum of any phylum detected at >1% of the total community. The dominant phyla in the core community are Proteobacteria and Acidobacteriota, similar to the total community.

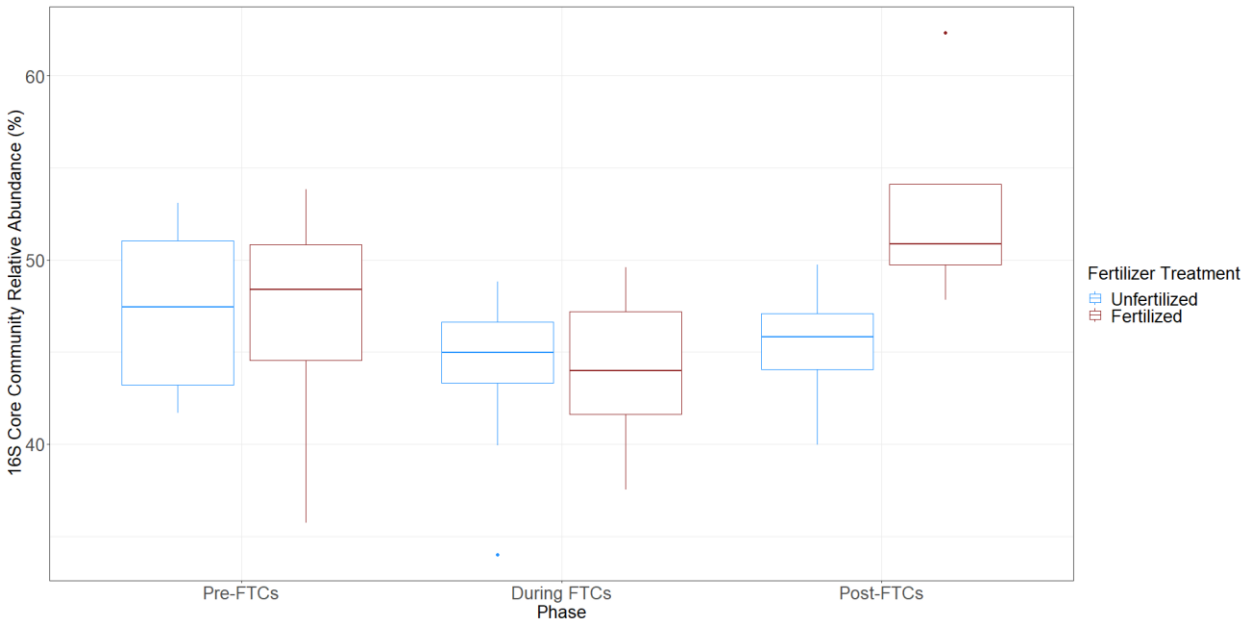

Figure 3.24: Bacterial and archaeal core community relative abundance over phase and fertilizer for the 5 cm depth. The total community relative abundance of the 94 ASVs identified for core community inclusion for just 5 cm depth samples were plotted over phase with fertilized and unfertilized treatments plotted separately. Tukey HSD tests for multiple pairwise comparisons identified significant differences associated only with fertilized columns pre- and post-FTCs, with a relative abundance difference of 8.9%.

The fungal core community also comprised 94 ASVs, from the 1,358 ASVs identified. The fungal core accounted for 70% of the total beta diversity, and made up a solid majority of the community, with approximately 80% of the relative abundance (Figure 3.25). The fungal core community abundance did not change significantly with fertilizer treatments or across phase (Figure 3.26). Its composition was dominated by the Ascomycota, as seen for the total community (Figure 3.27). The limited core fungal community response was also observed when the 5 cm depth samples were considered independently (Figure 3.28).

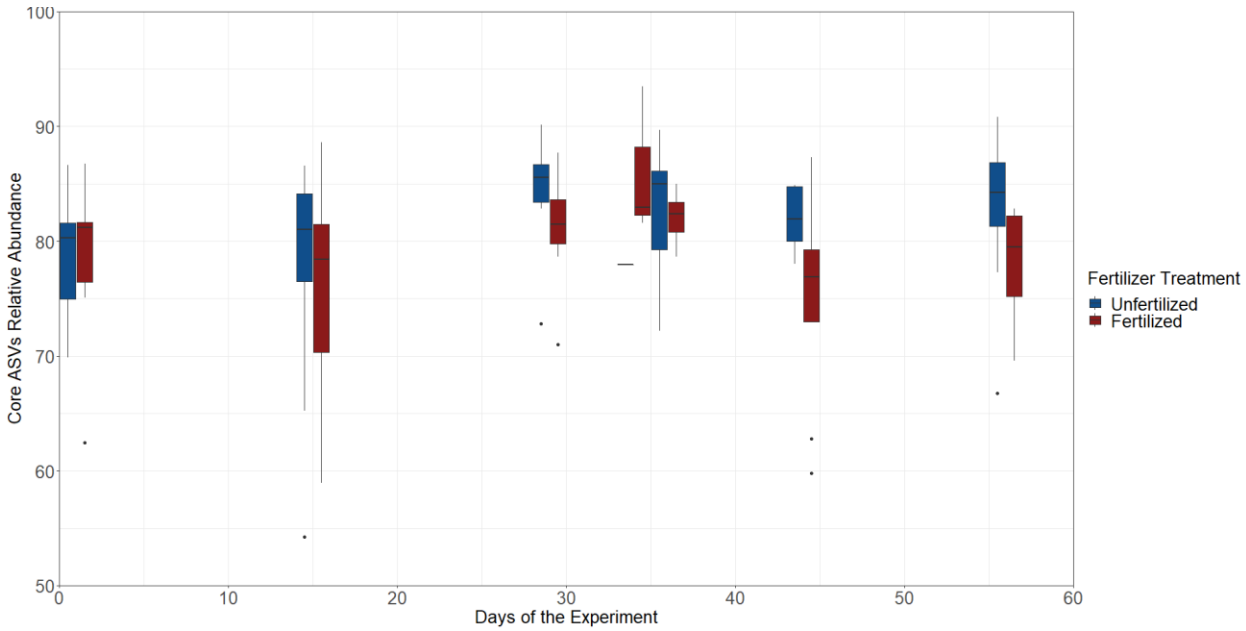

Figure 3.25: Fungal core community relative abundance over time and fertilizer. The total community relative abundance of the 94 ASVs identified for core community inclusion were plotted over time with fertilizer treatments plotted separately. Adjacent time-points and fertilizer treatments do not show significant variation. The core community appears unaltered in relative community abundance under freeze-thaw or nutrient induced stress.

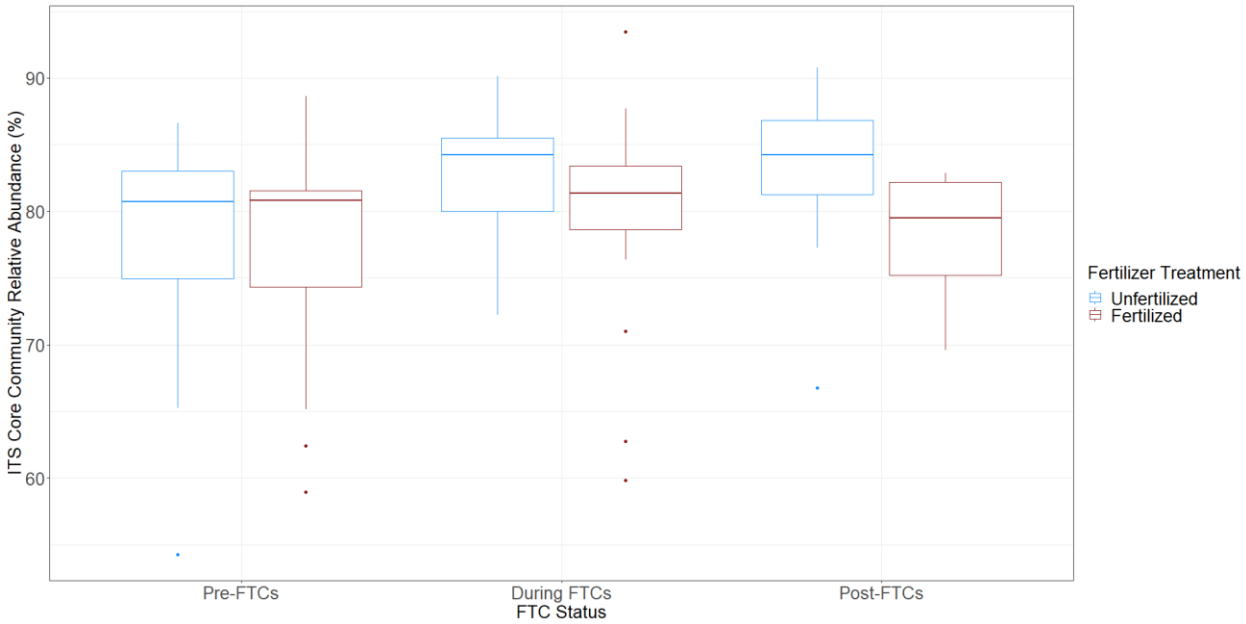

Figure 3.26: Fungal core community relative abundance over phase and fertilizer. The total community relative abundance of the 94 ASVs identified for core community inclusion were

plotted over phase with fertilized and unfertilized treatments plotted independently. Tukey HSD tests for multiple pairwise comparisons identified no significant differences between any of the fertilizer phase conditions with each other. The fungal core community appears unchanged in its relative abundance over the course of the experiment.

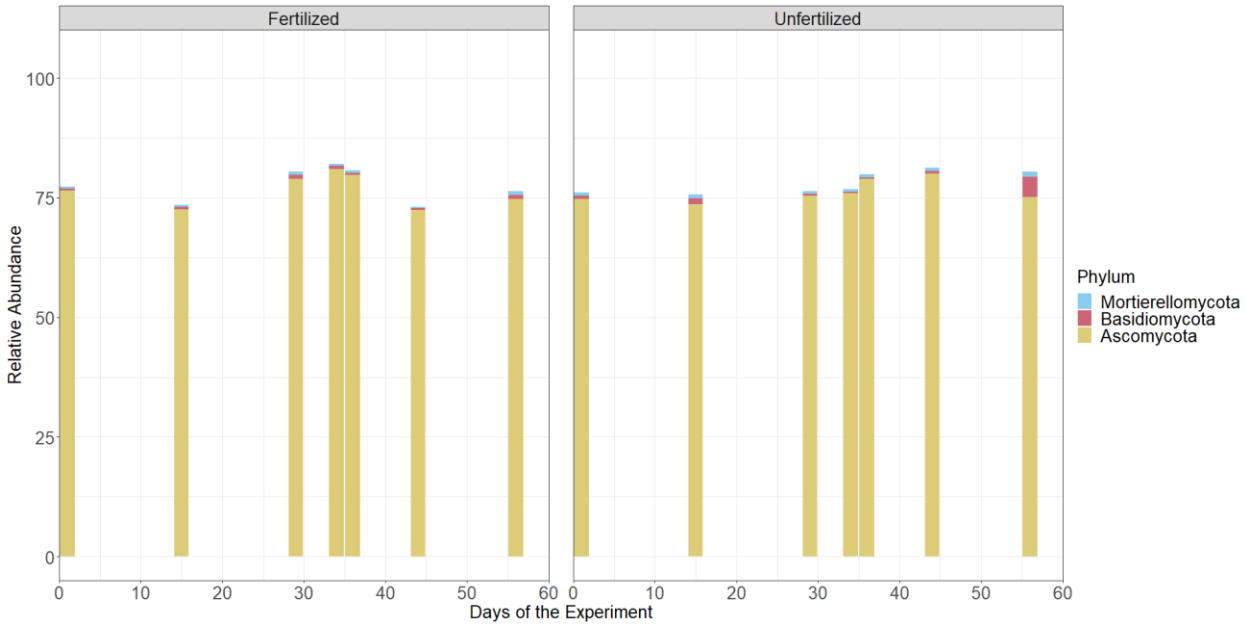

Figure 3.27: Fungal core community composition by major phyla over time with fertilizer treatments presented separately. The total community relative abundance of the 94 ASVs identified for core community inclusion were plotted over time and faceted across fertilizer treatments. The "Rare phyla" comprises the sum of any phylum detected at >1% of the total community. The dominant phylum in the fungal core community are Ascomycota, as was for the full community.

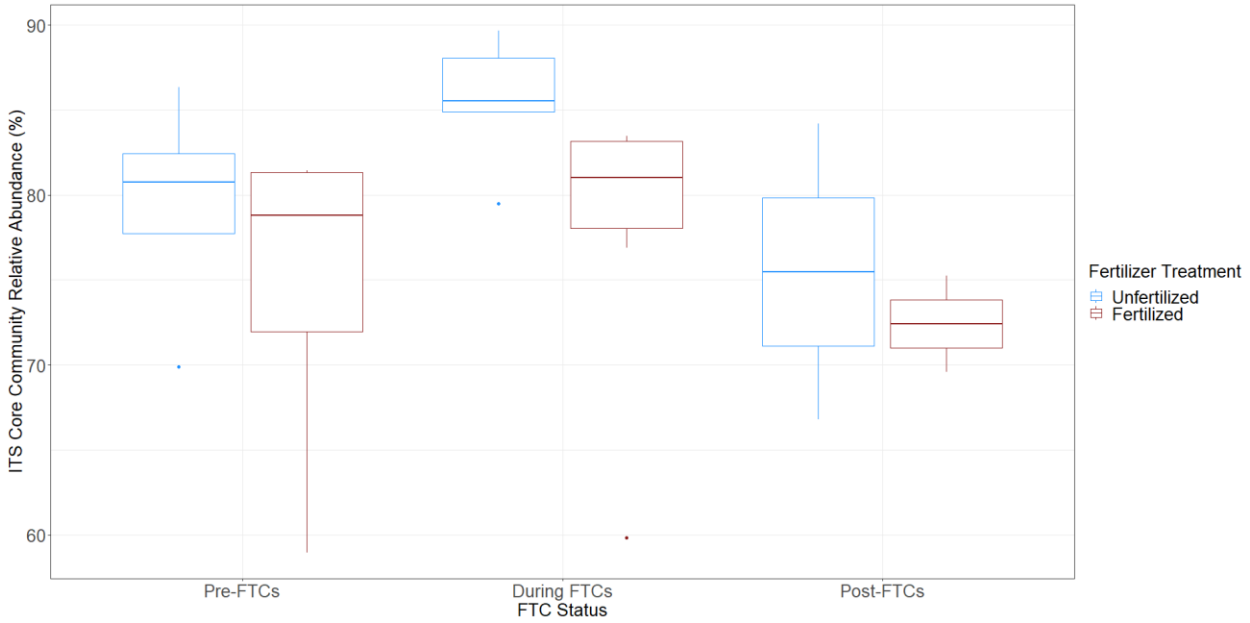

Figure 3.28: Fungal core community relative abundance over phase and fertilizer at 5 cm depth. The total community relative abundance of the 94 ASVs identified for core community inclusion for the 5 cm depth samples were plotted over phase with fertilized and unfertilized treatments plotted separately. Tukey HSD tests for multiple pairwise comparisons identified no significant differences between any of the fertilizer or phase conditions with each other. The 5 cm depth core fungal community appears similarly unchanged in its relative abundance despite nutrient and freeze-thaw stressors.

3.6 PICRUSt2 and Predicted Nitrogen Cycling Populations

PICRUSt2 was used to predict which ASVs in the bacterial and archaeal community are likely capable of nitrogen cycling based on their relationship to fully sequenced genomes annotated with EC numbers mediating conversion of nitrogen species (Douglas et al., 2020). Nitrogen cycling enzyme encoding genes included *ureC*, *amoA*, *hao*, *nxr*, *nar*, *nir*, *nor*, and *nosZ*, covering the key functions of the nitrification and denitrification pathways. The ASVs associated to each potential gene function were then combined into a single fraction of the total community's relative abundance and the resultant guilds tracked over time and between fertilizer treatments. Across the eight enzymes, there was little change in proportion across samples and between

fertilizer treatments (Figure 3.29). The ammonia oxidizing communities made up only a small fraction of the total community based on the predicted presence of *amoA* (~1% of community; Figure 3.30B), whereas the urea metabolizing community (i.e., potentially encoding *ureC*) made up ~25% of the community (Figure 3.30A). Tukey HSD multiple pairwise comparisons were used to determine significance across each unfertilized and fertilized pair per time-point. Tukey HSD multiple pairwise comparisons did not show significant differences broadly over time and fertilizer treatments with one exception. For the first sampling time point, 6 of the 8 explored enzymes have a significant enrichment in community abundance among fertilized samples compared to unfertilized samples (Figure 3.30C).

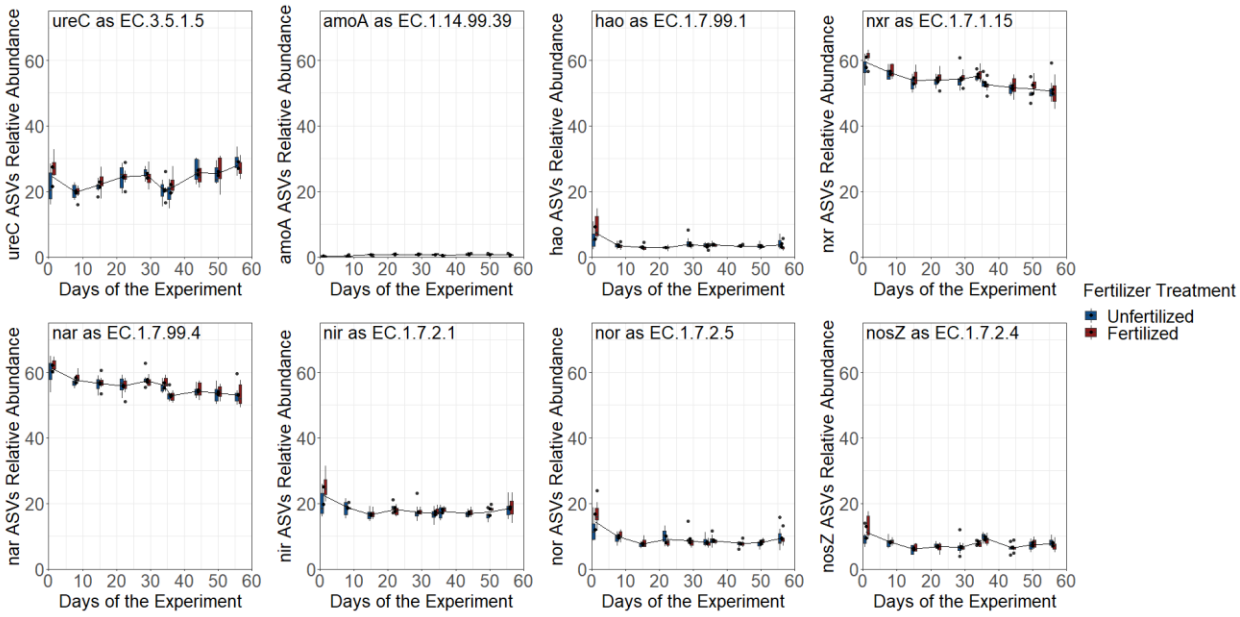

Figure 3.29: Predicted nitrogen cycling community relative abundance over time by enzyme classification number. Read counts for populations identified by PICRUSt2 to possess potential nitrogen cycling enzymes by EC number were combined to show the relative abundance of all populations in the community for each predicted enzyme class. Fertilizer treatments are presented separately.

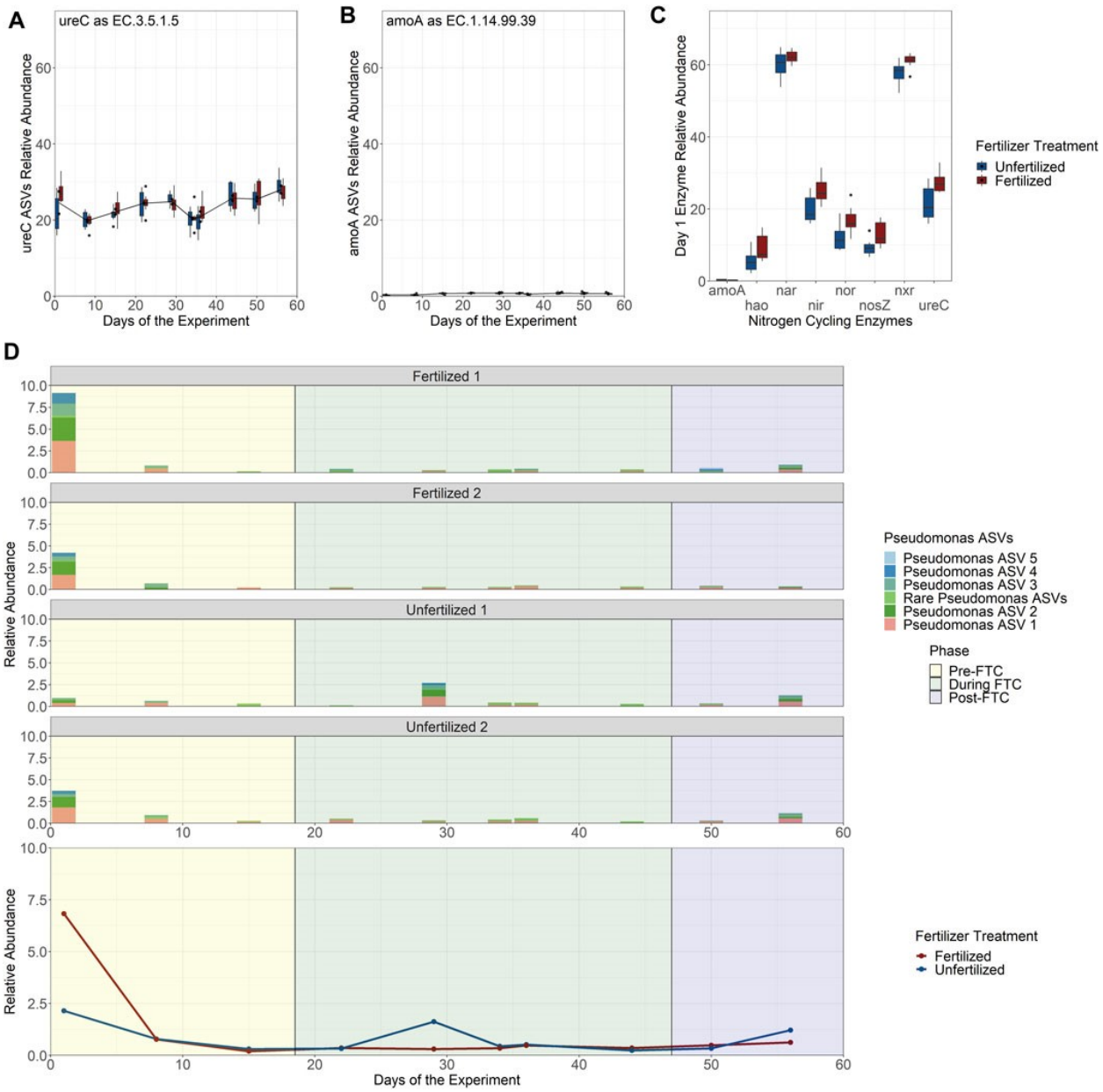

Figure 3.30: Predicted nitrogen cycling community relative abundance over time by enzyme classification number and *Pseudomonas* genus abundance contribution. (A–C) Read counts for populations identified by PICRUSt2 to possess potential nitrogen cycling enzymes by EC number were combined to show the relative abundance of all populations in the community for *ureC* (A) and *amoA* (B). Despite urea and ammonia being the primary constituents of the fertilizer there is little enrichment of the fertilized column treatments in predicted community members for their consumption with the exception of the first time-point (day 1) for 6 of the 8

investigated nitrogen cycling enzymes (C) that possess a statistically significant higher relative abundance among the fertilized treatments. This enrichment only exists on day 1 and is attributed to the ASVs belonging to the *Pseudomonas* genus. (D) The relative abundance of the *Pseudomonas* genus is shown over time separated by each experimental column with a breakdown of the *Pseudomonas* ASVs (the 5 most abundant numbered sequentially in their abundance; the remaining 10 ASVs are grouped together under "Rare *Pseudomonas* ASVs" with individual abundances of less than 0.15%) under the genus (top), and in aggregate across all columns (bottom).

Further exploration indicates that the enrichment in nitrogen cycling in fertilized columns on day 1 was associated with the *Pseudomonas* genus. Fifteen ASVs were assigned to *Pseudomonas,* with PICRUSt2 predicting that all fifteen should encode genes for *ureC*, *hao*, *nxr*, *nir*, *nor,* and *nosZ*. The relative abundance of *Pseudomonas* was then tracked over time between each column (Figure 3.30D: Top), where it starts at close to 10% relative abundance of the entire bacterial and archaeal community at the first sampling-point in the Fertilized 1 column. This early enrichment drops off after the initial nutrient spike at the beginning of the experiment, returning to levels seen in the other three columns over time (Figure 3.30D: Bottom). We predict that *Pseudomonas* is highly enriched under these conditions because the *Pseudomonas* are expected to be capable of multiple steps in nitrogen cycling and can extract energy from multiple nitrogen conversions (Arat et al., 2015), compared to the bulk of nitrogen cycling in soils which is uncoupled, with each step carried out by specific microbes.

Overall, this indicates that while unique microbes may be able to benefit from nutrient stress, the majority of microbial populations experience a muted change to biomass relative to the community. In this experiment, nutrient stress was not a strong selection event for microbes.

Chapter 4 Discussion

Northern temperate agricultural soils undergo broad environmental changes seasonally with freeze-thaw cycling through the non-growing season and increased nutrient load from pre-winter applied fertilizers. We hypothesized that environmental changes would act as selection events that would enrich for microbes with FTC resistance or opportunistic nitrogen cyclers. Instead, the results of this column experiment imply an alternative view, where seasonally experienced freeze-thaw cycles and fertilizer-induced nutrient load in agricultural soils are not significant stress events.

4.1 Freeze-Thaw Cycling as Regular Seasonal Changes

The experimental columns used in this experiment offered a more realistic agricultural soil microcosm than previous studies (Sulkava and Huhta, 2003; Koponen and Martikainen, 2004; Bechmann et al., 2005), utilizing a simulated climate model based on real data on a 1/3 timescale, artificial precipitation, and an insulated temperature gradient by depth. Frost heaving and freeze-thawing was achieved in soil columns despite using ambient temperatures no lower than −10°C and highs no higher than 10°C, following a diurnal frequency to mimic the rate of temperature change experienced by soil in nature (Henry, 2007). As a result, frost heaving of the topsoil was only observed at the shallowest depth. Under these conditions, bacterial, archaeal, and fungal communities did not exhibit strong compositional changes across the spatial or temporal variables examined. Across phase, an aggregate variable for extent of freeze-thaw cycling, changes in the relative abundances of taxa previously shown to respond to FTC were relatively muted. Significant decreases among the Acidobacteriota and Ascomycota phyla in all samples across experimental phase were less distinct and non-significant in the soil depth experiencing FTC, suggesting exposure to temperature fluctuations was not the main factor

driving these community shifts. This muted response in fungal communities to FTC, as evidenced by Ascomycota at consistently high proportional abundance, was expected, as their stable community composition has been observed previously (Sharma et al., 2006; Feng et al., 2007). The main exception to this community stability was the *Pseudomonas* genus across phase, which was later attributed to *Pseudomonas*'s predicted nitrogen cycling capacity. While we found change across the entire community to be minimal, the fungal community appeared particularly insulated at the phylum level with some distinct genera changes among the *Alternaria*, *Entoloma*, and *Staphylotrichum* (

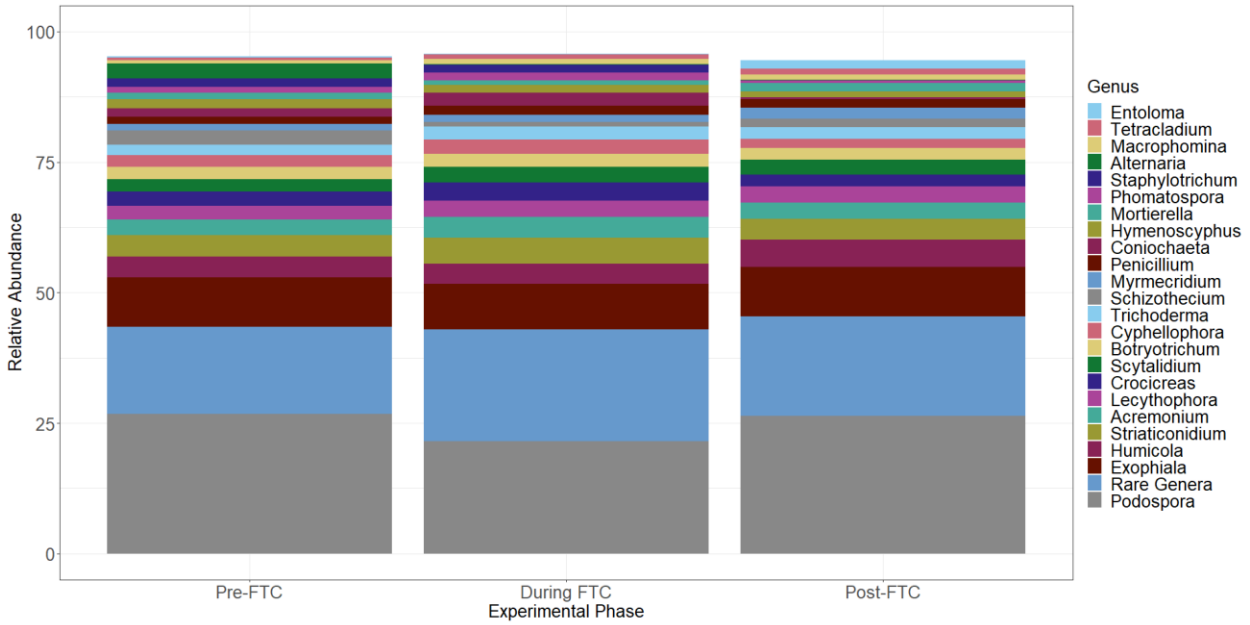

Figure 3.9). This resilience has been attributed previously to the role of fungal hyphae and greater substrate access (Schadt et al., 2003; Tucker et al., 2014).

For bacteria and archaea, alpha diversity metrics showed a clear pattern of increased diversity from pre-FTC to during FTC in the bacterial and archaeal community data, but with a return to previous diversity levels in the post-FTC phase. This change was significant and was observed at the shallowest depth. This trend sharply contrasts the expectation of a selection event leading to a

permanent change in the soil microbial community. The underlying cause of increased alpha diversity in the bacterial and archaeal community under FTC is not clear, with this elevated diversity present in all samples and not just the upper 5 cm depth directly experiencing FTC. We suggest two interpretations: 1) the eventual return of bacterial/archaeal alpha diversity to lower levels post-FTC implies a degree of community resilience to the stress of FTC, or 2) the change in alpha diversity is completely independent of FTC due to the stability of this trend at temperature insulated depths. In either case, FTC have limited impact on population abundances. FTC did not generate a site-specific community change in the shallowest depth, and, if responsible for the increased alpha diversities, resulted only in a temporary oscillation.

Investigation of beta diversity confirmed a community change in response to phase (but not to fertilizer or depth) (Figure 3.3). Canonical ordination mapping experimental variables to community variation showed clear separation of the samples based on phase (or analogs of it like days or time), with a significant magnitude of change. Despite the clear visual separation of the data by phase, only ~20% of the variation in the data was accounted for (Figure 3.19). Some geochemical variables were significant, but all had low coefficients of determination and did not explain much of the variation in the data. Taken together, this implies FTC have knock-on effects on communities at deeper, temperature-buffered depths, or that other, untested factors may play stronger roles in the bacterial/archaeal community compositional response.

Core community analysis assessed the response of microbial community members that are both spatially persistent and most abundant. Changes in the relative abundance of the core community, representing the persistent and abundant ASVs, would highlight the role of the non-persistent or stress induced ASVs on community resilience and cohesion. When the abundance of this core community was tracked over phase and fertilizer treatments (Figure 3.22), only

clustering samples by phase demonstrated variability, where, following an initial decrease during FTC, the bacterial and archaeal core community abundance recovers in the post-FTC phase. This corroborates the observed increase in alpha diversity during FTC for the total community, where the observed ~4–5% decrease in the core communities' relative abundance may represent novel populations displacing core populations in abundance. As this effect was more muted in the shallowest 5 cm depth, it is not clear these changes are the result of freeze-thaw cycling. Core community analyses indicated that the core community is relatively resilient, quickly recovering, and does not experience significant declines under what would conventionally be considered a stress event in the form of FTC. This has not commonly been observed in FTC literature, where the majority of studies have focused on arctic/permafrost soils, where active layer thawing gives rise to more dramatic changes to diversity and community compositions during freeze-thaw cycling (Deng et al., 2015; Müller et al., 2018; Yuan et al., 2018; Schostag et al., 2019). As northern temperate agricultural soils experience FTC seasonally for half the year, freeze-thaw cycling does not appear to act as a punctuated selection event. However, reliance on amplicon sequence data over truncated simulated timelines may obfuscate community changes due to sequencing of relic DNA, extracellular DNA in soil from dead cells, and may increase diversity estimates as much as 40% (Carini et al., 2016).

4.2 Fertilizer Nutrient Load as Temporary Enrichment

Two of the four experimental columns were amended with fertilizer to determine the impacts of nutrient load on the bacterial, archaeal, and fungal communities. Results from the flow-through leachate, as detailed in Krogstad et al. (2022), suggest significant fertilizer consumption, with NO_3^- increasing as the result of microbially-mediated nitrification processes. However, fertilizer was not found to be a significant variable explaining any of the observed variations of the

community composition, diversity, or core abundance, despite active microbially-mediated nitrification occurring over the experimental window (Krogstad et al. 2022). This was unexpected, as the ample supply of nitrogen and phosphorus provided by the fertilizer was expected to significantly enrich the fertilized communities for populations capable of nitrogen cycling.

The bacterial and archaeal communities did not exhibit strong compositional changes at the phylum level across the spatial, temporal, or fertilizer variables that were sampled. Lower taxonomic levels were also explored with no observable difference with respect to phase or fertilizer. We found that the bacterial/archaeal and fungal communities did not experience significant patterns in beta diversity associated with the fertilizer variable. In canonical ordinations, though the samples showed similar degrees of separation, no evident clustering based on fertilizer or other experimental variables was observed (Figure 3.17, Figure 3.18, Figure 3.20, Figure 3.21). Equally, the core community abundance did not show differences between the fertilized and unfertilized columns (Figure 3.22). Lack of stratification by depth in response to fertilizer amendment was expected, as Krogstad et al. (2022) demonstrated percolation of the dissolved fertilizer through the entire length of the column *via* the leachate. Therefore, the fertilizer was consumed throughout the entire column but did not contribute to differential growth. The implication is that fertilizer does not select for opportunistic growth but is merely consumed by existing, persistent members of the community. The impact on the microbial community is likely at the level of gene expression rather than population change.

A sole exception was the observation of significant enrichment of the *Pseudomonas* genus within one fertilized column in the first time point only, where the *Pseudomonas* were implicated in fertilizer-amended nitrogen cycling. However, this enrichment quickly collapses following the

first temporal sampling point. The implications of this observation are limited as it only appeared in one of the duplicate columns. The *Pseudomonas* may be enriched because they can leverage a greater degree of nitrogen utilization pathways. PICRUSt2 predicts this genus possesses *ureC*, *hao*, *nir*, *nxr*, *nar*, *nor*, and *nosZ*. We note inferences of function must be tempered as PICRUSt2 is only predicting gene potential. Some *Pseudomonas* are metabolically flexible, possessing both heterotrophic nitrification and aerobic (or facultative anaerobic) denitrification (Wei et al., 2021) in contrast to most nitrogen cyclers which have uncoupled nitrogen metabolisms, each with a specific niche (Palomo et al., 2018). The enrichment in *Pseudomonas* populations does not persist through later timepoints in the experiment and thus this brief enrichment does not appear to shape the microbial community.

Across other timepoints and conditions, the populations implicated in nitrogen metabolism, who would be expected to respond to fertilizer amendments, do not show significant change. Given active nitrification is occurring, these guilds are transforming nitrogen species, but this activity is not contributing to microbial growth. The window of fertilizer availability may not be prolonged enough to see differences in population abundances for microbes acting opportunistically in response to metabolic inputs. This is further evident by the extremely low relative abundance of putative ammonium monooxygenase-bearing populations in the total community despite ammonia conversion being an important early step to fertilizer assimilation. However, the high relative abundance of the putative urease-bearing population was not surprising as urea is often the end product of the metabolic breakdown of proteins, and its microbial conversion to ammonia is the primary mechanism for ammonia availability for plants (Witte, 2011).

Chapter 5 Conclusion and Recommendations

5.1 Microbial Community Changes from Environmental Stressors

From this experiment, freeze-thaw cycling and fertilizer amendments did not act as selection events nor cause significant changes to population abundances in agricultural soils over a simulated non-growing season. Rather than modeling these as stressors that alter the microbial community composition, we posit these are environmental conditions that are regularly experienced by the autochthonous microbial community. As a result, these do not cause significant changes to population abundances but may instead more strongly impact the community at the level of gene expression.

This contrasts with trends observed in arctic/permafrost soils, where active layer thawing creates clearly demarcated changes to microbial populations during freeze-thaw cycling (Deng et al., 2015; Han et al., 2018b; Müller et al., 2018; Mondini et al., 2019). The experimental columns used in this experiment generated a realistic agricultural soil microcosm, including real climate model data, simulated precipitation, and an insulated temperature gradient by depth. Other freeze-thaw studies have typically only sampled before and after seasons, whereas our longitudinal monitoring with interim sampling points allowed frequent sampling across depth, fertilizer treatment, and time for microbial community composition. Rather than assuming possible community changes may be reflective of binary states, this design explored the microbial communities' dynamics in near real time. The experimental design contributed to observing less dramatic microbial responses to FTC. However, there is still room for improvement including use of unfrozen controls, intact soil cores, more column replicates, removal of relic DNA, and active gene expression monitoring. Further experiments are needed to

assess the hypothesized expression level changes, ideally coupled to a holistic examination of community response including measurements of microbial biomass, activity, and composition.

5.2 Implications for Agricultural Best Management Practices

The results of this experiment indicate that freeze-thaw cycling has the potential to drastically reduce the potency of fertilizer applied pre-winter. Mineral fertilizer provides necessary nitrogen to agricultural crops in the form of urea and ammonia, but if consumed by opportunistic microorganisms during thaw events of FTC these crops may be deprived of essential nutrients. To compensate for this potential loss in potency, agricultural end-users with fields that experience seasonal freezing should modify their fertilizer regime in line with best management practices including the 4R Nutrient Stewardship guidelines (Johnston and Bruulsema, 2014).

For example, the Right Rate of fertilizer application can be adjusted by increasing the quantity of fertilizer applied to offset the loss from premature microbial consumption. The Right Time can be modified by applying fertilizer post-winter when applicable. The Right Place of fertilizer can be achieved through use of controlled-release fertilizers (to release nutrients gradually to limit consumption), and additives like nitrification inhibitors (to inhibit nitrifier metabolism).

Climate change may impact the agricultural productivity of seasonally frozen soils and industry must compensate to maintain production in the world of an increasing population.

References

Aanderud, Z. T., Jones, S. E., Schoolmaster, D. R., Fierer, N., and Lennon, J. T. (2013). Sensitivity of soil respiration and microbial communities to altered snowfall. *Soil Biol. Biochem.* 57, 217–227. doi:10.1016/j.soilbio.2012.07.022.

Arat, S., Bullerjahn, G. S., and Laubenbacher, R. (2015). A network biology approach to denitrification in Pseudomonas aeruginosa. *PLoS One* 10(2), 1-12. doi:10.1371/journal.pone.0118235.

Bechmann, M. E., Kleinman, P. J. A., Sharpley, A. N., and Saporito, L. S. (2005). Freeze-thaw effects on phosphorus loss in runoff from manured and catch-cropped soils. *J. Environ. Qual.* 34(6), 2301–2309. doi:10.2134/jeq2004.0415.

Bisanz, J. (2018). qiime2R: Importing QIIME2 artifacts and associated data into R sessions. Available at: https://github.com/jbisanz/qiime2R [Accessed March 17, 2022].

Boelter, D. H. (1972). Water table drawdown around an open ditch in organic soils. *J. Hydrol.* 15(4), 329–340. doi:10.1016/0022-1694(72)90046-7.

Bokulich, N. A., Kaehler, B. D., Rideout, J. R., Dillon, M., Bolyen, E., Knight, R., Huttley, G. A., Caporaso, J. G. (2018). Optimizing taxonomic classification of marker-gene amplicon sequences with QIIME 2's q2-feature-classifier plugin. *Microbiome* 6(1), 1-17. doi:10.1186/s40168-018-0470-z.

Bokulich, N. A., and Mills, D. A. (2013). Improved selection of internal transcribed spacer-specific primers enables quantitative, ultra-high-throughput profiling of fungal communities. *Appl. Environ. Microbiol.* 79(8), 2519–2526. doi:10.1128/aem.03870-12.

Bolyen, E., Rideout, J. R., Dillon, M. R., Bokulich, N. A., Abnet, C. C., Al-Ghalith, G. A., et al. (2019). Reproducible, interactive, scalable and extensible microbiome data science using QIIME 2. *Nat. Biotechnol.* 37(8), 852–857. doi:10.1038/s41587-019-0209-9.

Brooks, P. D., Williams, M. W., and Schmidt, S. K. (1998). Inorganic nitrogen and microbial biomass dynamics before and during spring snowmelt. *Biogeochemistry*, 43(1), 1-15. doi:10.1023/A:1005947511910.

Brown, P. J., and DeGaetano, A. T. (2011). A paradox of cooling winter soil surface temperatures in a warming northeastern United States. *Agric. For. Meteorol.,* 151(7), 947-956. doi:10.1016/j.agrformet.2011.02.014.

Burton, D. L., and Beauchamp, E. G. (1994). Profile nitrous oxide and carbon dioxide concentrations in a

soil subject to freezing. *Soil Sci. Soc. Am. J.,* 58(1), 115-122. doi:10.2136/sssaj1994.03615995005800010016x.

Callahan, B. J., McMurdie, P. J., Rosen, M. J., Han, A. W., Johnson, A. J. A., and Holmes, S. P. (2016). DADA2: High-resolution sample inference from Illumina amplicon data. *Nat. Methods* 13(7), 581–583. doi:10.1038/nmeth.3869.

CAPMoN (2018). Major Ions. *Environ. Clim. Chang. Canada*. Available at: http://donnees.ec.gc.ca/data/air/monitor/monitoring-ofatmospheric-precipitation-chemistry/major-ions/.

Carini, P., Marsden, P. J., Leff, J. W., Morgan, E. E., Strickland, M. S., and Fierer, N. (2016). Relic DNA is abundant in soil and obscures estimates of soil microbial diversity. *Nat. Microbiol.* 2(3), 1-6. doi:10.1038/nmicrobiol.2016.242.

Chantigny, M. H., Rochette, P., Angers, D. A., Goyer, C., Brin, L. D., and Bertrand, N. (2017). Nongrowing season N2O and CO2 emissions: temporal dynamics and influence of soil texture and fall-applied manure. *Can. J. Soil Sci.* 97(3), 452–464. doi:10.1139/CJSS-2016-0110.

Clarke, K. R. (1993). Non-parametric multivariate analyses of changes in community structure. *Aust. J. Ecol.* 18(1), 117–143. doi:10.1111/j.1442-9993.1993.tb00438.x.

Clein, J., and Schimel, J. (1995). Microibial activity of tundra and taiga soils at sub-zero temperatures. *Soil Biol. Biochem* 27(9), 1231–1234.

Conant, B. (2004). Delineating and quantifying ground water discharge zones using streambed temperatures. *Ground Water* 42(2), 243–257.

Deng, J., Gu, Y., Zhang, J., Xue, K., Qin, Y., Yuan, M., et al. (2015). Shifts of tundra bacterial and archaeal communities along a permafrost thaw gradient in Alaska. *Mol. Ecol.* 24(1), 222–234. doi:10.1111/mec.13015.

Douglas, G. M., Maffei, V. J., Zaneveld, J. R., Yurgel, S. N., Brown, J. R., Taylor, C. M., et al. (2020). PICRUSt2 for prediction of metagenome functions. *Nat. Biotechnol.* 38(6), 685–688. doi:10.1038/s41587-020-0548-6.

Du, E., Zhou, Z., Li, P., Jiang, L., Hu, X., and Fang, J. (2013). Winter soil respiration during soil-freezing process in a boreal forest in Northeast China. *J. Plant Ecol.* 6(5), 349–357. doi:10.1093/jpe/rtt012.

Feng, X., Nielsen, L. L., and Simpson, M. J. (2007). Responses of soil organic matter and microorganisms to freeze-thaw cycles. *Soil Biol. Biochem.* 39(8), 2027–2037. doi:10.1016/j.soilbio.2007.03.003.

Fierer, N. (2017). Embracing the unknown: Disentangling the complexities of the soil microbiome. *Nat. Rev. Microbiol.* 15(10), 579–590. doi:10.1038/nrmicro.2017.87.

Funk, G., McClenaghan, W., and Holland, C. (1980). Water wells and ground water supplies in Ontario, Ontario Ministry of the Environment Report ISBN 0-7743-5072-5. Toronto, Ontario Available at: https://atrium.lib.uoguelph.ca/server/api/core/bitstreams/79f06ce7-e6ed-4934-90d4-1b2e13524bf6/content.

Gasser, J. K. R. (1958). Use of deep-freezing in the preservation and preparation of fresh soil samples. *Nature* 181, 1334–1335.

Gee, G. W., and Bauder, J. W. (1986). "Particle-size analysis," in *Methods of Soil Analysis: Part 1 Physical and Mineralogical Methods*, ed. A. Klute (Madison, Wisconsin, USA: American Society of Agronomy), 383–411. doi:10.2136/sssabookser5.1.2ed.c15.

Graham, D. E., Wallenstein, M. D., Vishnivetskaya, T. A., Waldrop, M. P., Phelps, T. J., Pfiffner, S. M., et al. (2012). Microbes in thawing permafrost: the unknown variable in the climate change equation. *ISME J.*, 6(4), 709-712. doi:10.1038/ismej.2011.163.

Hall, E. K., Singer, G. A., Kainz, M. J., and Lennon, J. T. (2010). Evidence for a temperature acclimation mechanism in bacteria: an empirical test of a membrane-mediated trade-off. *Funct. Ecol.,* 24(4), 898-908. doi:10.1111/j.1365-2435.2010.01707.x.

Han, C. L., Gu, Y. J., Kong, M., Hu, L. W., Jia, Y., Li, F. M., et al. (2018a). Responses of soil microorganisms, carbon and nitrogen to freeze–thaw cycles in diverse land-use types. *Appl. Soil Ecol.* 124, 211–217. doi:10.1016/j.apsoil.2017.11.012.

Han, Z., Deng, M., Yuan, A., Wang, J., Li, H., and Ma, J. (2018b). Vertical variation of a black soil's properties in response to freeze-thaw cycles and its links to shift of microbial community structure. *Sci. Total Environ.* 625, 106–113. doi:10.1016/j.scitotenv.2017.12.209.

Hayashi, M. (2014). The cold vadose zone: hydrological and ecological significance of frozen-soil processes. *Vadose Zo. J.* 13(1), 1-8. doi:10.2136/vzj2013.03.0064er.

Henry, H. A. L. (2007). Soil freeze-thaw cycle experiments: Trends, methodological weaknesses and suggested improvements. *Soil Biol. Biochem.* 39(5), 977–986. doi:10.1016/j.soilbio.2006.11.017.

Herrmann, A., and Witter, E. (2002). Sources of C and N contributing to the flush in mineralization upon freeze-thaw cycles in soils. *Soil Biol. Biochem.* 34(10), 1495–1505. doi:10.1016/S0038-0717(02)00121-9.

Herzog, S., Wemheuer, F., Wemheuer, B., and Daniel, R. (2015). Effects of fertilization and sampling

time on composition and diversity of entire and active bacterial communities in German grassland soils. *PLoS One* 10(12), 1–20. doi:10.1371/journal.pone.0145575.

Ivarson, K. C., and Sowden, F. J. (1970). Effect of frost action and storage of soil at freezing temperatures on the free aminoa acids, free sugars and respiratory activity of soil. *Canadian Journal of Soil Science,* 50(2), 191-198. Available at: www.nrcresearchpress.com.

Johnston, A. M., and Bruulsema, T. W. (2014). 4R nutrient stewardship for improved nutrient use efficiency. *Procedia Engineering,* 83, 365-370. doi:10.1016/j.proeng.2014.09.029.

Kassambara, A. (2020). ggpubr: "ggplot2" Based Publication Ready Plots. Available at: https://rpkgs.datanovia.com/ggpubr/ [Accessed March 17, 2022].

Koponen, H. T., and Martikainen, P. J. (2004). Soil water content and freezing temperature affect freeze-thaw related N2O production in organic soil. *Nutr. Cycl. Agroecosystems* 69(3), 213–219. doi:10.1023/B:FRES.0000035172.37839.24.

Krogstad, K., Gharasoo, M., Jensen, G., Hug, L. A., Rudolph, D., Van Cappellen, P., Rezanezhad, F. (2022). Nitrogen leaching from agricultural soils under imposed freeze-thaw cycles: a column study with and without fertilizer amendment. *Front. Environ. Sci.,* 10. doi:10.3389/fenvs.2022.915329

Kuzyakov, Y., and Blagodatskaya, E. (2015). Microbial hotspots and hot moments in soil: concept & review. *Soil Biol. Biochem.,* 83, 184-199. doi:10.1016/j.soilbio.2015.01.025.

Larsen, K. S., Ibrom, A., Jonasson, S., Michelsen, A., and Beier, C. (2007). Significance of cold-season respiration and photosynthesis in a subarctic heath ecosystem in Northern Sweden. *Glob. Chang. Biol.,* 13(7), 1498-1508. doi:10.1111/j.1365-2486.2007.01370.x.

Lipson, D. A., Monson, R. K., Scmidt, S. K., and Weintraub, M. N. (2009). The trade-off between growth rate and yield in microbial communities and the consequences for under-snow soil respiration in a high elevation coniferous forest. *Biogeochemistry* 95, 23–35. doi:10.1007/s10533-008-9252-1.

Mack, A. R. (1963). Biological activity and mineralization of nitrogen in three soils as induced by freezing and drying. *Can. J. Soil Sci.* 43(2), 316–324. Available at: www.nrcresearchpress.com.

Martin, M. (2011). Cutadapt removes adapter sequences from high-throughput sequencing reads. *EMBnet J.* 17(1), 10–12.

Matzner, E., and Borken, W. (2008). Do freeze-thaw events enhance C and N losses from soils of different ecosystems? A review. *Eur. J. Soil Sci.* 59(2), 274–284. doi:10.1111/j.1365-2389.2007.00992.x.

McMurdie, P. J., and Holmes, S. (2013). Phyloseq: an R package for reproducible interactive analysis and graphics of microbiome census data. *PLoS One* 8(4), 1-11. doi:10.1371/journal.pone.0061217.

Mondini, A., Bang-Andreasen, T., Anwar, M. Z., and Purcarea, C. (2019). Total RNA protocol (extraction, quantification and Illumina library preparation). doi:10.17504/protocols.io.457gy9n.

Müller, O., Bang-Andreasen, T., White, R. A., Elberling, B., Taş, N., Kneafsey, T., et al. (2018). Disentangling the complexity of permafrost soil by using high resolution profiling of microbial community composition, key functions and respiration rates. *Environ. Microbiol.* 20(12), 4328-4342. doi:10.1111/1462-2920.14348.

Nikrad, M. P., Kerkhof, L. J., and Häggblom, M. M. (2016). The subzero microbiome: microbial activity in frozen and thawing soils. *FEMS Microbiol. Ecol.* 92(6), 1–16. doi:10.1093/femsec/fiw081.

Nilsson, R. H., Larsson, K. H., Taylor, A. F. S., Bengtsson-Palme, J., Jeppesen, T. S., Schigel, D., et al. (2019). The UNITE database for molecular identification of fungi: handling dark taxa and parallel taxonomic classifications. *Nucleic Acids Res.* 47(D1), D259–D264. doi:10.1093/nar/gky1022.

Oksanen, J., Blanchet, G., Friendly, M., Kindt, R., Legendre, P., McGlinn, D., et al. (2019). vegan: community ecology package. Available at: https://github.com/vegandevs/vegan [Accessed March 17, 2022].

Palomo, A., Pedersen, A. G., Fowler, S. J., Dechesne, A., Sicheritz-Pontén, T., and Smets, B. F. (2018). Comparative genomics sheds light on niche differentiation and the evolutionary history of comammox Nitrospira. *ISME J.* 12(7), 1779–1793. doi:10.1038/s41396-018-0083-3.

Pesaro, M., Widmer, F., Nicollier, G., and Zeyer, J. (2003). Effects of freeze-thaw stress during soil storage on microbial communities and methidathion degradation. *Soil Biol. Biochem.,* 35(8), 1049-1061. doi:10.1016/S0038-0717(03)00147-0.

Quast, C., Pruesse, E., Yilmaz, P., Gerken, J., Schweer, T., Yarza, P., et al. (2013). The SILVA ribosomal RNA gene database project: Improved data processing and web-based tools. *Nucleic Acids Res.* 41(D1), 590–596. doi:10.1093/nar/gks1219.

Ren, J., Song, C., Hou, A., Song, Y., Zhu, X., and Cagle, G. A. (2018). Shifts in soil bacterial and archaeal communities during freeze-thaw cycles in a seasonal frozen marsh, Northeast China. *Sci. Total Environ.* 625, 782–791. doi:10.1016/j.scitotenv.2017.12.309.

Rivkina, E. M., Friedmann, E. I., McKay, C. P., and Gilichinsky, D. A. (2000). Metabolic activity of Permafrost Bacteria below the freezing point. *Appl. Environ. Microbiol.* 66(8), 3230–3233. doi:10.1128/AEM.66.8.3230-3233.2000.

Romero, C. M., Engel, R. E., Chen, C., Wallander, R., and Jones, C. A. (2017). Late-fall, winter, and spring broadcast applications of urea to no-till winter wheat II. fertilizer N recovery, yield, and protein as affected by NBPT. *Soil Sci. Soc. Am. J.* 81(2), 331. doi:10.2136/sssaj2016.10.0333.

Röver, M., Heinemeyer, O., and Kaiser, E. A. (1998). Microbial induced nitrous oxide emissions from an arable soil during winter. *Soil Biol. Biochem.,* 30(14), 1859-1865. doi:10.1016/S0038-0717(98)00080-7.

RStudio Team (2020). RStudio: integrated development for R. Available at: http://www.rstudio.com/ [Accessed March 17, 2022].

Schadt, C. W., Martin, A. P., Lipson, D. A., and Schmidt, S. K. (2003). Seasonal dynamic of previously unknown fungal lineages in tundra soils. *Science,* 301(5638), 1359–1361. doi:10.1016/S1359-6454(03)00232-5.

Schmidt, S. K., and Lipson, D. A. (2004). Microbial growth under the snow: implications for nutrient and allelochemical availability in temperate soils. *Plant Soil*., 259, 1-7. doi:10.1023/B:PLSO.0000020933.32473.7e.

Schostag, M., Priemé, A., Jacquiod, S., Russel, J., Ekelund, F., and Jacobsen, C. S. (2019). Bacterial and protozoan dynamics upon thawing and freezing of an active layer permafrost soil. *ISME J.* 13(5), 1345–1359. doi:10.1038/s41396-019-0351-x.

Schuur, E. A. G., McGuire, A. D., Schädel, C., Grosse, G., Harden, J. W., Hayes, D. J., et al. (2015). Climate change and the permafrost carbon feedback. *Nature*, 520, 171-179. doi:10.1038/nature14338.

Shade, A., and Stopnisek, N. (2019). Abundance-occupancy distributions to prioritize plant core microbiome membership. *Curr. Opin. Microbiol.* 49, 50–58. doi:10.1016/j.mib.2019.09.008.

Sharma, S., Szele, Z., Schilling, R., Charles, J., Schloter, M., Sharma, S., et al. (2006). Influence of freeze-thaw stress on the structure and function of microbial communities and denitrifying populations in soil influence of freeze-thaw stress on the structure and function of microbial communities and denitrifying populations in soil. *Appl. Environ. Microbiol.* 72(3), 2148–2154. doi:10.1128/AEM.72.3.2148.

Soulides, D., and Allison, F. (1961). Effect of drying and freezing soils on carbon dioxide production, available mineral nutrients, aggregation, and bacterial population. *Soil Sci.* 91(5), 291–298.

Sulkava, P., and Huhta, V. (2003). Effects of hard frost and freeze-thaw cycles on decomposer communities and N mineralisation in boreal forest soil. *Appl. Soil Ecol.* 22(3), 225–239.

doi:10.1016/S0929-1393(02)00155-5.

Taş, N., Prestat, E., McFarland, J. W., Wickland, K. P., Knight, R., Berhe, A. A., et al. (2014). Impact of fire on active layer and permafrost microbial communities and metagenomes in an upland Alaskan boreal forest. *ISME J.,* 8(9), 1904-1919. doi:10.1038/ismej.2014.36.

Teepe, R., Brumme, R., and Beese, F. (2001). Nitrous oxide emissions from soil during freezing and thawing periods. *Soil Biol. Biochem.* 33(9), 1269–1275. doi:10.1016/S0038-0717(01)00084-0.

Tucker, C. L., Young, J. M., Williams, D. G., and Ogle, K. (2014). Process-based isotope partitioning of winter soil respiration in a subalpine ecosystem reveals importance of rhizospheric respiration. *Biogeochemistry* 121(2), 389-408. doi:10.1007/s10533-014-0008-9.

Walker, V. K., Palmer, G. R., and Voordouw, G. (2006). Freeze-thaw tolerance and clues to the winter survival of a soil community. *Appl. Environ. Microbiol.,* 72(3), 1784-1792. doi:10.1128/AEM.72.3.1784-1792.2006.

Walters, W., Hyde, E. R., Berg-Lyons, D., Ackermann, G., Humphrey, G., Parada, A., et al. (2015). Improved bacterial 16S rRNA gene (V4 and V4-5) and fungal internal transcribed spacer marker gene primers for microbial community surveys. *mSystems* 1(1), 1-10. doi:10.1128/msystems.00009-15.

Watanabe, K., and Osada, Y. (2017). Simultaneous measurement of unfrozen water content and hydraulic conductivity of partially frozen soil near 0 °C. *Cold Reg. Sci. Technol.* 142(August 2015), 79–84. doi:10.1016/j.coldregions.2017.08.002.

Wei, R., Hui, C., Zhang, Y., Jiang, H., Zhao, Y., and Du, L. (2021). Nitrogen removal characteristics and predicted conversion pathways of a heterotrophic nitrification–aerobic denitrification bacterium, Pseudomonas aeruginosa P-1. *Environ. Sci. Pollut. Res.* 28(6), 7503–7514. doi:10.1007/s11356-020-11066-7.

Wickham, H. (2016). *ggplot2: elegant graphics for data analysis*. Springer-Verlag New York Available at: https://ggplot2.tidyverse.org [Accessed March 17, 2022].

Wickham, H., François, R., Henry, L., and Müller, K. (2021). dplyr: A grammar of data manipulation. Available at: https://github.com/tidyverse/dplyr [Accessed March 17, 2022].

Witte, C. (2011). Urea metabolism in plants. *Plant Science* 180(3), 431-438. doi:10.1016/j.plantsci.2010.11.010.

Yanai, Y., and Toyota, K. (2005). Effects of soil freeze-thaw cycles on microbial biomass and organic matter decomposition, nitrification and denitrification potential of soils. in *Proc. Int. Symp. of JSPS*

Core to Core Program between Hokkaido University and Martin Luther University Symptom of Environmental Change in Siberian Permafrost Region (Halle-Wittenberg). doi:10.1080/00380768.2004.10408542.

Yuan, M. M., Zhang, J., Xue, K., Wu, L., Deng, Y., Deng, J., et al. (2018). Microbial functional diversity covaries with permafrost thaw-induced environmental heterogeneity in tundra soil. *Glob. Chang. Biol.* 24(1), 297–307. doi:10.1111/gcb.13820.

Zhang, T. (2005). Influence of the seasonal snow cover on the ground thermal regime: an overview. *Rev. Geophys.* 43(4), 1-23. doi:10.1029/2004RG000157.

Zhang, T., Barry, R. G., Knowles, K., Ling, F., and Armstrong, R. L. (2003). Distribution of seasonally and perennially frozen ground in the Northern Hemisphere. *Proceedings of the 8th International Conference on Permafrost*, 2, 1289-1294.

Žifčáková, L., Větrovský, T., Howe, A., and Baldrian, P. (2016). Microbial activity in forest soil reflects the changes in ecosystem properties between summer and winter. *Environ. Microbiol.* 18(1), 288–301. doi:10.1111/1462-2920.13026.